Surface Science 603 (2009) 3104–3118

Contents lists available at ScienceDirect

Surface Science

journal homepage: www.elsevier.com/locate/susc

Hydrogen desorption kinetics and band bending for 6H–SiC(0 0 0 1) surfaces

S.W. King [a,*], R.F. Davis [a,1], R.J. Nemanich [b,2]

[a] Department of Materials Science and Engineering, North Carolina State University, Raleigh, NC 27695-7907, United States
[b] Department of Physics, North Carolina State University, Raleigh, NC 27695-8202, United States

ARTICLE INFO

Article history:
Received 23 February 2009
Accepted for publication 24 August 2009
Available online 29 August 2009

Keywords:
Silicon carbide
Hydrogen
Temperature programmed desorption
Kinetics

ABSTRACT

The desorption kinetics of hydrogen from polished 6H–SiC(0 0 0 1) surfaces exposed to various sources of hydrogen have been determined using temperature programmed desorption (TPD). For (3 × 3) 6H–SiC(0 0 0 1) surfaces prepared via annealing and cooling in SiH_4, desorption of 0.2 ± 0.05 monolayer of molecular hydrogen was observed to occur at ≈590 °C. This β_1 H_2 desorption peak exhibited second order kinetics with an activation energy of 2.4 ± 0.2 eV. For (3 × 3) 6H–SiC surfaces exposed to atomic hydrogen generated via either a hot rhenium filament or remote hydrogen plasma, low energy electron diffraction patterns showed an eventual conversion back to (1 × 1) symmetry. Spectra acquired using Auger electron and X-ray photoelectron spectroscopies revealed that the atomic hydrogen exposure removed the excess Si. Photoelectron spectroscopy results also showed a 0.5 eV increase in binding energy for the Si2p and C1s core levels after removal of the Si–Si bilayer that is indicative of a decrease in band bending at the SiC surface. TPD from the (3 × 3) 6H–SiC(0 0 0 1) surfaces exposed to atomic hydrogen showed substantially more molecular hydrogen desorption (1–2 ML) through the appearance of a new desorption peak ($\beta_{2,3}$) that started at ≈200 °C. The $\beta_{2,3}$ peak exhibited second order desorption kinetics and a much lower activation energy of 0.6 ± 0.2 eV. A third smaller hydrogen desorption state was also detected in the 650–850 °C range. This last feature could be resolved into two separate desorption peaks (α_1 and α_2) both of which exhibited second order kinetics with activation energies of 4.15 ± 0.15 and 4.3 ± 0.15 eV, respectively. Based on comparisons to hydrogen desorption from Si and diamond surfaces, the β and α desorption peaks were assigned to hydrogen desorption from Si and C sites, respectively.

1. Introduction

Hydrogen is prevalent throughout most semiconductor electronic device fabrication steps including epitaxial thin film crystal growth [1–3], reactive ion etching [4,5], wet chemical surface cleaning and etching [6–8], plasma cleaning [9–11], chemical mechanical polishing [12–14], contact formation/metallization [15–17], and passivating interface states/electrical defects [18–20]. For SiC in particular, hydrogen is one of the few known etchants for this material [21,22]. Most recently, annealing in hydrogen has also become a popular method for preparing silicon carbide surfaces for III-N hetero-epitaxial growth [23,24] and numerous studies characterizing (0 0 0 1) 6H–SiC surfaces prepared in this fashion have been reported [25–33]. Additional studies have focused on the structure of hydrogen terminated (0 0 1) 3C–SiC surfaces [34–37], hydrogen passivation of dangling bonds/surface states on polar (0 0 1) 3C–SiC [38–42] and (0 0 0 1) 6H–SiC [29,31,33] surfaces, and non-polar $(1\bar{1}00)$ and $(11\bar{2}0)$ 4H–SiC surfaces [43], and atomic hydrogen induced reconstructions on (0 0 1) 3C–SiC [38,39] and (0 0 0 1) 6H–SiC surfaces [44–48]. However, only a few detailed studies investigating the kinetics of atomic or molecular hydrogen adsorption [49,50] and desorption [51–53] from SiC surfaces have been reported. This is in contrast to the numerous studies reported concerning the adsorption and desorption of hydrogen from the surfaces of the two elements which comprise SiC–Si [54–84] and C [85–116].

For Si it has been well established that molecular hydrogen at room temperature has essentially a zero sticking coefficient ($S \leqslant 10^{-8}$) on terraces [54] and a similarly near negligible initial sticking coefficient ($S_0 \approx 10^{-4}$) on vicinal surfaces where molecular hydrogen adsorption has been shown to be enhanced at surface steps [55]. Atomic hydrogen generated via cracking over a hot filament, however, has been observed to have an initial sticking coefficient (S_0) of 1 and follow an $S = 1 - \text{coverage}\ (\theta)$ relationship [56]. On the (2 × 1) Si(1 0 0) reconstructed surface, atomic hydrogen adsorbs primarily in the monohydride state up to a coverage of 1

* Corresponding author. Present address: Portland Technology Development, Intel Corporation, Hillsboro, OR 97124, United States. Tel.: +1 503 613 7547; fax: +1 971 214 7811.
E-mail addresses: sean.king@intel.com (S.W. King), rfd@andrew.cmu.edu (R.F. Davis), Robert.Nemanich@asu.edu (R.J. Nemanich).
[1] Present address: Department of Materials Science and Engineering, Carnegie Mellon University, 5000 Forbes Avenue, Pittsburgh, PA 15213-3890, United States. Tel.: +1 412 268 7264.
[2] Present address: Department of Physics, Arizona State University, P.O. Box 871504, Tempe, AZ 85287-1504, United States. Tel.: +1 480 965 2240.

0039-6028/$ - see front matter © 2009 Elsevier B.V. All rights reserved.
doi:10.1016/j.susc.2009.08.023

monolayer (ML = 6.78 × 10^{14} atom/cm^2). At higher hydrogen coverage, the (2 × 1) surface reconstruction converts to (3 × 1) due to Si–Si dimer cleavage and dihydride formation. At a saturation coverage of 1.8–2.0 ML, trihydride species form on the (1 0 0) surface and the surface symmetry converts to (1 × 1) [57–62]. On the (7 × 7) Si(1 1 1) surface, atomic hydrogen is likewise observed to initially adsorb primarily in a monohydride state up to a coverage of 0.3 monolayer (ML = 7.8 × 10^{14} atoms/cm^2 for Si(1 1 1)) at which point the surface converts to a (1 × 1) low energy electron diffraction (LEED) pattern and dihydride and trihydride formation occurs until a saturation coverage of 1.1–1.5 ML is achieved [62–65].

Monohydride desorption from Si(1 1 1) surfaces is observed to exhibit second order kinetics with reported activation energies ranging from 2.4–2.7 eV [56,68–72]. In contrast, monohydride desorption from the Si(1 0 0) surface is observed to exhibit first order kinetics, and with slightly lower activation energies ranging from 2.0 to 2.5 eV [70,72–82] (see Table 1 for a summary of the reported hydrogen desorption kinetics from Si surfaces). The observed second order desorption kinetics from the Si(1 1 1) surface is consistent with a recombinatory desorption mechanism for randomly positioned hydrogen atoms, while the first order kinetics observed for the Si(1 0 0) surface has been attributed to recombinatory desorption of two hydrogen atoms paired on the same silicon dimer on the (2 × 1) Si(1 0 0) surface. The lower activation energies for H_2 desorption from the Si(1 0 0) surface (2.0–2.3 eV) are primarily observed from Si(1 0 0) surfaces hydrogenated by exposure to SiH_4, Si_2H_6 or Si_3H_8 [68–82,84]. For Si(1 1 1) and Si(1 0 0) surfaces hydrogenated by exposure to atomic hydrogen generated by a hot tungsten filament, the activation energy for H_2 desorption for both surfaces is generally observed to be in the range of 2.5–2.9 eV [56,69–72,75,76]. Desorption of dihydride species from the various Si surfaces have been reported to exhibit 0.8–1.2 eV lower activation energies relative to the monohydride state and a mix of first and second order desorption kinetics have been reported [56,71,83].

For diamond and graphite surfaces, molecular hydrogen is also observed to have a near zero sticking/adsorption coefficient at room temperature whereas atomic hydrogen readily adsorbs on these surfaces [85–87]. For the (2 × 1) C(1 0 0) surface, atomic hydrogen is observed to adsorb exclusively in a monohydride state up to saturation coverage [87,88] with no change in the (2 × 1) surface symmetry [90–92]. Dihydride formation on the (1 0 0) surface is believed to occur only at steps or other surfaces defects [89]. The inability to form dihydrides at higher coverage is attributed to steric hindrance effects arising due to the close proximity of dihydrides on the smaller diamond surface lattice [93,94]. Reports of conversion of the (2 × 1) C(1 0 0) surface to (1 × 1) symmetry with large atomic hydrogen exposures [85,95,96] are attributed to roughening of the C(1 0 0) surface by repeated atomic hydrogen

Table 1
Reported activation energies and pre-exponentials for hydrogen desorption from various silicon surfaces.

Orientation	Specie	Coverage (ML)	Order	E_d (eV)	ν_d (ν_2 cm^2/s) (ν_1 s^{-1})	Method	Ref.
Si(1 1 1)	H_2	NS	Second	1.7 ± 0.15	0.03	Flash TPD	[66]
Si(1 1 1)	H_2	NS	Second	1.9 ± 0.3	0.05	Flash TPD	[66]
(2 × 1) Si(1 1 1)	H_2-β_1	≪1	Second	2.54 ± 0.1	136	TPD	[56]
(2 × 1) Si(1 1 1)	H_2-β_1	1	Second	3.5	10^8	TPD	[56]
(2 × 1) Si(1 1 1)	H_2-β_2	>1	First	1.9±0.3	NS	NS	[56]
(7 × 7) Si(1 1 1)	H_2	<1	Second	2.65 ± 0.17	1.2 ± 0.13	LITD	[68]
(7 × 7) Si(1 1 1)	D_2	<1	Second	2.56 ± 0.13	2.8 ± 1	LITD	[68]
(7 × 7) Si(1 1 1)	H_2	0.7	Second	2.61 ± 0.17	3	TPD	[68]
(7 × 7) Si(1 1 1)	H_2	0.4	Second	2.39 ± 0.22	0.25	TPD	[68]
(7 × 7) Si(1 1 1)	H_2	0.25	Second	2 ± 0.21	0.0012	TPD	[68]
(7 × 7) Si(1 1 1)	H_2	0.3–0.7	Second	2.69 ± 0.17	91	LITD	[70]
(7 × 7) Si(1 1 1)	H_2	0.1–0.8	Second	2.74 ± 0.21	231	TPD	[70]
(7 × 7) Si(1 1 1)	H_2	NS	NS	1.5	0.01	SHG	[69]
(7 × 7) Si(1 1 1)	H_2	0.08–0.14	1.56	2.4	6 × 10^{13}	I-SHG	[69]
(7 × 7) Si(1 1 1)	D_2-β_{1A}	0.05–1.25	Second	2.5 ± 0.1	2	TPD	[71,72]
(7 × 7) Si(1 1 1)	D_2-β_{1B}	0.05–1.25	Second	2.45 ± 0.1	1	TPD	[71,72]
(2 × 1) Si(1 1 1)	D_2-β_2	>0.7	Second	2.0 ± 0.1	0.5	TPD	[71,72]
Si(1 0 0)	H_2-β_1	0.1–0.5	First	2.04	7.9 × 10^{11}	I-LITD	[73,74]
Si(1 0 0)	D_2-β_1	0.1–0.5	First	2.04	5.6 × 10^{11}	I-LITD	[73,74]
Si(1 0 0)	H_2-β_1	0.1–1	First	2.17 ± 0.09	2.2 × 10^{12}	TPD	[73,74]
Si(1 0 0)	H_2-β_1	0.006–1	First	1.95 ± 0.09	2.2 × 10^{11}	I-LITD	[73,74]
Si(1 0 0)	D_2-β_1	0.006–1	First	1.95 ± 0.09	1.3 × 10^{11}	I-LITD	[73,74]
(2 × 1) Si(1 0 0)	H_2	0.1–1	First	2.52 ± 0.09	5.5 × 10^{15}	LITD	[70]
(2 × 1) Si(1 0 0)	H_2	0.1–1	First	2.87 ± 0.17	6.5 × 10^{17}	TPD	[70]
(2 × 1) Si(1 0 0)	H_2	>0.1	First	2.48 ± 0.1	2 × 10^{15}	I-SHG	[75]
(2 × 1) Si(1 0 0)	D_2-β_1	0.05–1.5	First	2.50	2 × 10^{15}	TPD	[76]
(2 × 1) Si(1 0 0)	D_2-β_2	>1	Second	2.00	4.4	TPD	[76]
(2 × 1) Si(1 0 0)	H_2	NS	First	2.25 ± 0.15	6 × 10^{13}	SDR	[78]
Si(1 0 0)	H_2	0.1–1	First	2.3 ± 0.04	9 ± 2 × 10^{13}	TPD	[80,81]
Si(1 0 0)	H_2	NS	First	2.1 ± 0.04	6 ± 4 × 10^{13}	TPD	[80,81]
Si(1 0 0)	H_2	NS	First	2.1 ± 0.1	8 ± 1 × 10^{13}	TPD	[80,81]
Si(1 0 0)	H_2	NS	First	2.2 ± 0.05	3.7 ± 2.8 × 10^{13}	SHG	[82]
(2 × 1) Si(1 0 0)	H_2	0.1–1	First	2.48 ± 0.1	2.2 ± 1 × 10^{15}	LITD	[79]
Si(1 0 0)	H_2	0.1–1	First	2.35 ± 0.1	2.32 ± 1 × 10^{14}	LITD	[79]
(2 × 1) Si(1 0 0)	H_2	NS	First	2.2 ± 0.2	3.4 ± 0.3 × 10^{13}	STM	[77]
Poly/amor	H	NS		1.82 ± 0.06	NS	NS	[67]
Porous Si	H_2	NS	Second	2.82	170	I-FTIR	[83]
Porous Si	H_2	NS	Second	1.86	0.047	I-FTIR	[83]
(7 × 7) Si(1 1 1)	SiH_3	NS	First	1.35 ± 0.09	10^{10}	SSIMS	[84]

NS = not specified, LITD = laser induced thermal desorption, SHG = second harmonic generation, I = isothermal, SDR = surface differential reflectance, STM = scanning tunneling microscopy, poly/amor = polycrystalline/amorphous.

exposures [11,92]. In contrast, atomic hydrogen adsorption on the (2×1) C(1 1 1) surface is observed to convert the surface symmetry back to (1×1) symmetry [97,98]. As is the case for the C(1 0 0) surface, essentially only monohydride species are observed on the hydrogen saturated C(1 1 1) surface [99–102].

Similar to the Si(1 0 0) surface, hydrogen desorption from the C(1 0 0) surface has been observed to be first order with reported activation energies ranging from 1.6 to 4.1 eV [85,88,91–93,95,96]. Hydrogen desorption from the C(1 1 1) surface and poly-crystalline diamond surfaces have also been reported to be first order with activation energies in the range of 2.9–4 eV [98,103–106] (see Table 2 for a summary of hydrogen desorption kinetics from various diamond surfaces). The former is in contrast to results from Si(1 1 1) where second order kinetics has been reported. It is also in contrast with results from spectroscopic and pyrolytic grade graphites and a:C–H where second order kinetics have been reported with desorption activation energies ranging from 0.7 to 2.5 eV [87,107–114] (see Table 3 for a summary of hydrogen desorption kinetics from various graphite and a-C:H surfaces). The observed first order hydrogen desorption kinetics from C(1 1 1) surfaces have been attributed to segregation and formation of hydrogen surface domains vs. the random adsorption of hydrogen attributed to the second order kinetics for the Si(1 1 1) surface [98]. Graphite has also been reported to be a catalyst for the recombination of atomic H [115,116].

For silicon carbide, molecular hydrogen has also been observed to effectively have a zero sticking coefficient at room temperature ($S_0 < 10^{-6}$) [49,51]. Although for the $c(4 \times 2)$ 3C–SiC(1 0 0) surface, Derycke et al. [49] have reported a relatively small but significant initial room temperature sticking coefficient (S_0) of 2×10^{-3}. The enhanced adsorption for molecular hydrogen on this surface is attributed to the presence of undulating dimer rows on the $c(4 \times 2)$ surface with adsorption specifically occurring at step like up-dimer sites (similar to Si(1 0 0) surfaces where molecular hydrogen adsorption is observed to be enhanced by surface steps). For the silicon rich (3×2) 3C–SiC surface which lacks undulating dimer rows, Derycke et al. reports the sticking coefficient for molecular hydrogen to be effectively zero. However, annealing 6H–SiC(0 0 0 1) substrates in molecular hydrogen at higher temperatures (1000–1100 °C) has been shown to generate well ordered hydrogen terminated surfaces [25–32]. At these temperatures, it is not clear whether the hydrogen termination is the result of the increased reactivity of molecular H_2 with (0 0 0 1) surfaces or due to the generation of small amounts of atomic H. Fourier transform infra-red–attenuated total reflection spectroscopy (FTIR–ATR) has clearly shown this procedure does generate surfaces terminated by silicon monohydrides for the $(0\,0\,0\,1)_{Si}$ surface and carbon monohydrides species for the $(0\,0\,0\,\bar{1})_C$ surface [25–32]. At this point, it should be noted that 6H–SiC(0 0 0 1) surfaces are structurally equivalent to 3C–

Table 2
Reported activation energies and pre-exponentials for hydrogen desorption from various diamond surfaces.

Orientation	Specie	Coverage (ML)	Order	E_d (eV)	ν_d (ν_2 cm^2/s) (ν_1 s^{-1})	Method	Ref.
(2×1) C(1 0 0)	H_2	<0.38	First	1.6	3×10^5	TPD	[85]
(2×1) C(1 0 0)	H_2	NS	First	3.15	10^{13}	TPD	[90]
(2×1) C(1 0 0)	H_2	NS	First	3.45	10^{13}	TPD	[88]
C(1 0 0)	D_2	NS	First	3.1	10^{13}	TPD	[95]
(2×1) C(1 0 0)	H_2	NS	First	1.7 ± 0.6	$3.2 \pm 0.7 \times 10^5$	I-SDR	[91]
(2×1) C(1 0 0)	D_2	NS	First	3.8	10^{13}	TPD	[96]
(2×1) C(1 0 0)	H_2	NS	First	3.5 ± 0.06	1.4×10^{13}	TPD	[98]
(2×1) C(1 0 0)	H_2	NS	Second	3.3 ± 0.02	2.3×10^{13}	TPD	[98]
(2×1) C(1 0 0)	D_2	α	First	3.5 ± 0.06	$1.4 \pm 0.9 \times 10^{13}$	TPD	[98]
(2×1) C(1 0 0)	D_2	β	Second	3.3 ± 0.02	$2.3 \pm 0.9 \times 10^{13}$	TPD	[98]
$(2 \times 2)/(2 \times 1)$ C(1 1 1)	D_2	β_1-0.5	First	3.5	5×10^{12}	TPD	[103]
$(2 \times 2)/(2 \times 1)$ C(1 1 1)	D_2	β_2	First	2.9	5×10^{12}	TPD	[103]
(1×1) C(1 1 1)	D_2	0.2–1	First	3.7 ± 0.1	$9.5 \pm 4 \times 10^{13}$	TPD	[98]
(2×1) C(1 1 1)	D_2	0.1–1.0	First	4 ± 0.4	$10^{15\pm2}$	I-SFG	[99]
CVD Poly diamond	H_2	0.1–1	First	3.0 ± 0.3	$10^{10.5\pm0.9}$	I-TOF-SARS	[105,106]
CVD Poly diamond	D_2	0.1–1	First	3.0 ± 0.3	$10^{10.5\pm0.9}$	I-TOF-SARS	[105,106]
Arc jet poly diamond	D_2	0.26–0.57	First	2.2	5×10^7	TPD	[104]

SFG = Sum frequency generation, TOF-SARS = Time of flight scattering and recoil spectroscopy.

Table 3
Reported activation energies and pre-exponentials for hydrogen desorption from various graphite and amorphous carbon surfaces.

Orientation	Specie	Coverage	Order	E_d (eV)	ν_d (ν_2 cm^2/s) (ν_1 s^{-1})	Exp Method	Ref.
Prism	H_2	NS	NS	0.7	1.06×10^{-2}	MMBMS	[107]
Basal	H_2	NS	NS	0.8	1.3×10^{-4}	MMBMS	[107]
Basal	H_2	NS	Second	1.15	NS	TPD	[87]
NS	H_2	NS	Second	1.9	3×10^{-7}	TPD	[109]
NS	CD_4	NS	First	1.65	6×10^8	TPD	[109]
NS	D_2	NS	Second	2.5	10^{13}	TPD	[108]
NS	D_2	NS	Second	3.5	10^{13}	TPD	[108]
NS	H_2	NS	NS	1.2	10^{13}	TPD	[110]
NS	CH_4	NS	NS	2.3	10^{13}	TPD	[110]
NS	H_2	NS	NS	0.8	NS	TPD	[111]
NS	CH_4	NS	NS	1.8	NS	TPD	[111]
a-C:H	H_2	NS	First	2.86	NS	TPD	[113]
a-C:H	CH_4	NS	First	2.47	NS	TPD	[113]
a-C:H	C_2H_4	NS	NS	2.2	NS	TPD	[112]
a-C:H	C_2H_6	NS	NS	2.2	NS	TPD	[112]
a-C:H	H_2	NS	NS	2.7	NS	TPD	[114]

SiC(1 1 1) surfaces and differ only in the Si–C stacking sequence starting at the fourth Si–C bilayer below the surface [28]. Also both 3C–SiC(1 1 1) and 6H–SiC(0 0 0 1) surfaces are polar and can be either carbon or silicon terminated. SiC(1 1 1)/(0 0 0 1) surfaces further differ from silicon and carbon (1 1 1) surfaces in that the three back bonds for surface silicon or carbon atoms are not homopolar Si–Si or C–C bonds but heteropolar Si–C bonds [26].

Similar to silicon and diamond surfaces, atomic hydrogen is observed to have a near unity sticking coefficient at room temperature and induce significant surface changes on adsorbing to SiC [38–42,45–48]. For the (0 0 1) 3C–SiC surface, room temperature adsorption of atomic hydrogen has been observed to convert the (3×2) and $c(4 \times 2)$ surfaces to (3×1) and (2×1) surface periodicity respectively [39,40]. Multiple internal reflection infra-red absorption spectroscopy indicates that the hydrogenated (3×2)/(3×1) and $c(4 \times 2)$/(2×1) surfaces consist predominantly of silicon monohydride species with some dihydride species present on the $c(4 \times 2)$ surface but perhaps limited in concentration by the presence of repulsive interactions between hydrogen atoms on adjacent Si–Si dimers [41,42]. For $(0\,0\,0\,1)_{Si}$ 6H–SiC surfaces, room temperature atomic hydrogen adsorption has been observed to convert (3×3) and $(\sqrt{3} \times \sqrt{3})$ surfaces into (1×1) surface periodicity [45,46,50]. For the $(\sqrt{3} \times \sqrt{3})$ surface, Fujino et al. [46] have determined using time-of-flight elastic recoil detection analysis that the hydrogen coverage saturates at about 1.7 ML (ML = 1.4×10^{15} atom/cm^2 for (0 0 0 1) 6H–SiC). For the (3×3) surface, the high resolution electron energy loss spectroscopy (HREELS) experiments by Stoldt et al. [50] indicate that for the 6H–SiC(0 0 0 1) surface, the (3×3) to (1×1) conversion by atomic hydrogen exposure is the result of atomic hydrogen etching/removal of the extra Si bilayer that creates the (3×3) surface reconstruction. Similar selective silicon removal has been inferred by Aoyama et al. [47,48] for $(\sqrt{3} \times \sqrt{3})$ surfaces exposed to atomic hydrogen. Interestingly, this is in contrast to studies of the (3×2) 3C–SiC(0 0 1) surface which contains an extra Si monolayer and for which no Si etching by atomic hydrogen exposure was reported [39].

Concerning hydrogen desorption from SiC surfaces, multiple studies report that annealing at temperatures >700–900 °C results in hydrogen desorption from both the (0 0 1) 3C–SiC and (0 0 0 1) 6H–SiC surfaces with an accompanying restoration of the pre-hydrogen surface symmetry/LEED pattern [33,39,40,45–47]. Regarding the kinetics of hydrogen desorption, Allendorf and Outka [51] detected two first order desorption states (E_d = 2.7 and 3.1 eV) in temperature programmed desorption (TPD) spectra acquired from sputter cleaned poly-crystalline CVD β-SiC. Due to the wide surface heterogeneity present on the poly-crystalline samples, Allendorf and Outka were unable to definitively assign a desorption state to a particular surface specie. Kim and Olander [52] subsequently utilized modulated molecular beam mass spectrometry to study atomic hydrogen etching of poly-crystalline SiC surfaces and determined SiH_4, CH_4, and C_2H_2 to be the main reaction products from 300 to 1100 K. Based on these measurements, they deduced extremely low activation energies of 0.03 and 0.06 eV for the reaction probability of forming the former two species. It should be noted that SEM inspection of the poly-crystalline surfaces indicated atomic hydrogen attack of the SiC surface occurred primarily at the grain boundaries. Additional studies have been performed investigating hydrogen desorption from a-SiC:H thin films and various forms of poly-crystalline and single crystalline SiC implanted with high energy hydrogen ions (see Table 4 for summary of reported H_2 desorption kinetics from SiC surfaces). These studies have reported a wide range of 0.7–4.0 eV for hydrogen desorption activation energies from SiC and attributed the H_2 desorption to a wide variety of surface and sub-surface species/traps [117–122]. More detailed information could be obtained from studying the desorption of thermally generated atomic hydrogen from well characterized single crystalline SiC surfaces. However to the author's knowledge, such studies do not appear to have been reported in the literature.

Due to the prevalence and importance of hydrogen in SiC materials processing and the lack of investigations of hydrogen desorption from well ordered single crystalline surfaces, we have attempted to investigate the kinetics of hydrogen desorption from (0 0 0 1) 6H–SiC surfaces using TPD, LEED, Auger electron spectroscopy (AES), and X-ray photoelectron spectroscopy (XPS). The results confirm prior reports of preferential etching of excess Si from (3×3) 6H–SiC(0 0 0 1) surfaces by atomic hydrogen and indicate second order desorption kinetics for hydrogen desorption from (0 0 0 1)6H–SiC surfaces of varying surface structure and stoichiometry. Based on the determined activation energies for desorption and the measured surface stoichiometry, hydrogen desorption is concluded to occur from both Si and C sites with activation energies consistent with those observed from Si and diamond surfaces.

2. Experimental

The substrates and the sample preparation procedures used in these experiments have been described in detail elsewhere [123–125]; however, a brief overview is presented herein. The polished, off-axis (4° toward $(11\bar{2}0)$), n-type ($N_d = 10^{18}$/cm^3), 6H–SiC(0 0 0 1) 1″ diameter substrates were acquired from Cree, Inc. These substrates were ultrasonically rinsed in acetone and metha-

Table 4
Reported activation energies and pre-exponentials for hydrogen desorption from various SiC surfaces.

Orientation	Specie	Coverage (ML)	Order	E_d (eV)	ν_d (ν_2 cm^2/s) (ν_1 s^{-1})	Method	Ref.
CVD Poly 3C–SiC	H_2	0.05–3	First	2.7	10^{13}	TPD	[51]
CVD Poly 3C–SiC	H_2	0.05–3	First	3.1	10^{13}	TPD	[51]
CVD Poly 3C–SiC	H_2	0.05–3	First	1.5	10^{7}	TPD	[51]
CVD Poly 3C–SiC	H_2	NS	First	0.03	4.6×10^{2}	MMBMS	[52]
CVD Poly 3C–SiC	H_2	NS	First	0.06	5.4×10^{2}	MMBMS	[52]
CVD Poly 3C–SiC	D_2	Implanted	NS	2.3 ± 0.5	NS	TPD	[121]
CVD Poly 3C–SiC	D_2	Implanted	NS	3.12 ± 0.17	NS	TPD	[121]
CVD Poly 3C–SiC	D_2	Implanted	NS	3.7 ± 0.76	NS	TPD	[121]
α-SiC	H_2	Implanted	First	4 ± 0.2	NS	TPD	[118]
Poly α-SiC	D_2	Implanted	Second	0.7 ± 0.3	NS	IsoAnnl	[120]
a-SiC:H	H_2	Bulk	First	1.63	NS	TPD	[117]
(3×3) 6H–SiC(0 0 0 1)	H_2-β_1	0.2 ± 0.05	Second	2.4 ± 0.2	$10^{-1\pm0.5}$	TPD	This work
(3×3) 6H–SiC(0 0 0 1)	H_2-$\beta_{2,3}$	1.4–2.4	Second	0.55 ± 0.15	$3 \times 10^{-14\pm1}$	TPD	This work
(1×1) 6H–SiC(0 0 0 1)	H_2-$\beta_{2,3}$	0.55 ± 0.05	Second	0.75 ± 0.15	$6 \times 10^{-12\pm1}$	TPD	This work
(1×1) 6H–SiC(0 0 0 1)	H_2-α_1	0.1 ± 0.05	Second	4.15 ± 0.15	$2 \times 10^{5\pm1}$	TPD	This work
(1×1) 6H–SiC(0 0 0 1)	H_2-α_2	0.1 ± 0.05	Second	4.35 ± 0.15	$2 \times 10^{5\pm1}$	TPD	This work

IsoAnnl = isothermal annealling.

nol, exposed to the vapor from a 10:1 buffered HF solution for 10 min, mounted to a molybdenum sample holder using tantalum wire, and immediately loaded into an ultra-high vacuum (UHV) transfer line [126] having a base pressure of 9×10^{-10} Torr. This line connected to the TPD/III-N gas source molecular beam epitaxy (GSMBE) system, the LEED unit, the XPS system, the AES system, and the remote hydrogen plasma system used in this research. The capabilities of these UHV systems have been detailed elsewhere [127].

Hydrogenated 6H–SiC(0 0 0 1) surfaces were prepared by three different methods. The first consisted of annealing a 6H–SiC(0 0 0 1) surface in $10^{-5} - 10^{-6}$ Torr SiH_4 for ≈15–20 min at 950–1050 °C and then cooling to <200 °C before stopping the SiH_4 flow. This procedure generated oxygen free 6H–SiC(0 0 0 1) surfaces with a (3×3) reconstruction which has been shown to consist of a full Si–Si bilayer on top of the 6H–SiC surface [125]. These (3×3) 6H–SiC(0 0 0 1) surfaces were believed to be hydrogen terminated by analogy to experiments performed on Si(1 0 0) surfaces which have shown that hydrogen termination remains after 523 °C SiH_4 exposure and quenching to room temperature [80]. In the latter two methods, (1×1) and (3×3) 6H–SiC surfaces prepared by the above SiH_4 anneal procedure were exposed to atomic hydrogen generated either via thermal cracking over a hot rhenium filament (≈1700 °C) or via exposure to a remote H_2 plasma. For the former, exposures were performed in 10^{-6} Torr H_2 with the sample 3.5 inches from the filament. Radiative heating of the sample was not observed to increase the surface temperature beyond 100 °C, and this slight increase in surface temperature was not believed to significantly impact the results reported herein. Remote H_2 plasma exposures were performed at 450 °C and ~40 cm downstream from a 13.56 MHz inductively coupled H_2 plasma. The H_2 plasma was operated at 20 W and 15 mTorr. At this pressure, the plasma was largely confined upstream of the sample, but a weak diffuse glow was observed in the sample vicinity. Prior characterization of the H_2 plasma has shown it to consist primarily of H, H^+, H_2, and electrons. H_2 to H dissociation efficiencies and H^+/H ratios of 50% and 10^{-4}, respectively have been previously estimated for these plasma conditions. The energy of the ions in the plasma is low with an average characteristic energy of ~223 °C. Further details of the remote H_2 plasma treatment are described elsewhere [9]. Unhydrogenated (1×1) and (3×3) 6H–SiC(0 0 0 1) surfaces were generated by H_2 desorption during TPD experiments performed on SiH_4 annealed surfaces. These unhydrogenated surfaces were also exposed to the above two atomic hydrogen sources.

The TPD experiments were conducted in the GSMBE system using a Hiden Analytical 0–200 amu quadrapole mass spectrometer fitted inside a differentially pumped chamber having a 0.5 cm diameter opening. The sample holder/heater was positioned in front of this opening. The opening was located <2.5 cm from the sample surface. The TPD experiments were conducted to a maximum temperature of 1200 °C using a heating rate of 30–60 °C/min while sampling m/e^- 2, 12, and 28 with the quadrapole mass spectrometer. To ensure that the desorption features detected originated only from the 6H–SiC sample and not from the sample holder or heater, several additional TPD experiments were conducted. First as the TPD sample heater was exposed to SiH_4 and H/H_2 during the SiH_4 clean and hot filament atomic hydrogen dosing, the sample heater was always independently degassed prior to any TPD measurements. The degas procedure consisted of loading a separate sample holder containing a blank molybdenum disk and heating to 1200 °C for >5 min. TPD spectra collected from the blank Mo disk after this degassing procedure showed an essentially flat H_2 signal up to 1000 °C and was taken as the baseline H_2 background for the heater in these experiments. To further confirm that the detected H_2 signal was coming from the sample, TPD spectra were collected from both a hydrogenated SiC sample and hydrogenated molybdenum disk but with the sample/heater rotated 180° from the QMS chamber. In these experiments, only a small linear rise in H_2 signal was observed indicating that the amount of H_2 detected in our TPD experiments from non line of sight desorbing H_2 was minimal. Lastly to rule out H_2 desorption from the Mo sample holder and Ta mounting wires, TPD spectra were collected from Si(1 1 1) and poly-crystalline Mo disks exposed to the same SiH_4 and atomic hydrogen sources. The spectra collected from these surfaces were compared to those collected from the SiC surfaces to ensure that the desorption features detected were unique to the SiC sample and not the Mo sample holder and tantalum mounting wire. In this regard, it is also important to note that the SiC samples utilized in these experiments were 2.54 cm in diameter whereas the opening to our mass spectrometer chamber was only 0.5 cm in diameter. This geometry helped to minimize the amount of line of sight H_2 desorption from the Mo sample holder and Ta mounting wire that could make it into the mass spectrometer chamber.

Additional spurious effects may also occur in TPD experiments such as electron stimulated desorption (ESD) of H caused by electrons from the mass spectrometer ionizer. While enclosing the mass spectrometer in the differentially pumped chamber may help to minimize this effect, we were not able to independently bias the chamber opening to completely eliminate it. Thus some ESD effects may be present in our data. However, we feel this effect would only contribute to our background H_2 signal and not significantly alter our conclusions.

To calibrate the hydrogen desorption signal from the 6H–SiC(0 0 0 1) surfaces, hydrogen desorption from a (7×7) Si(1 1 1) surface exposed to a saturation dose of atomic hydrogen from the hot rhenium filament was also examined (see Fig. 1). The saturation surface coverage of hydrogen from a Si(1 1 1) surface has been previously determined to be 1.25 monolayer (ML = $7.8 \times 10^{14}/cm^2$) by Culbertson et al. [65]. By equilibrating the area under the H_2 TPD spectra from a saturated Si(1 1 1) surface to $9.75 \times 10^{14}/cm^2$, we were able to calibrate against a known standard the intensity of the desorption peaks from our 6H–SiC(0 0 0 1) H_2 TPD spectra. The boron doped (0.8–1.2 Ω cm), chemomechanically polished, on-axis Si(1 1 1) wafers were obtained from Virginia Semiconductor, Inc. The (7×7) Si(1 1 1) surface was prepared by heating the sample to 900 °C in $<1 \times 10^{-9}$ Torr in the TPD/GSMBE system.

Kinetic treatments of TPD spectra normally use the Polanyi–Wigner desorption rate equation [128,129]:

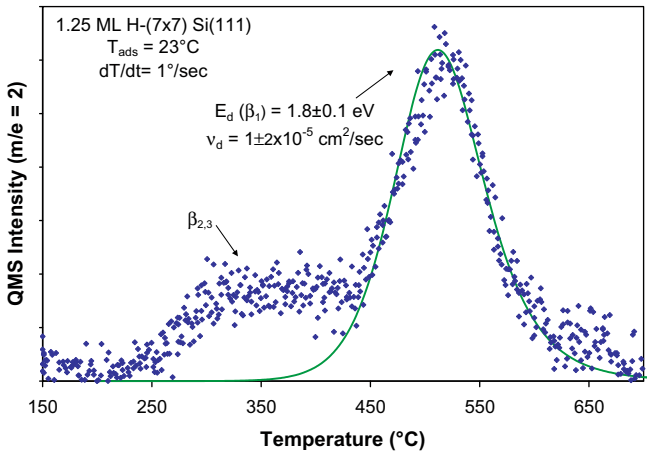

Fig. 1. H_2 (m/e^- = 2) TPD spectrum from a (7×7) Si(1 1 1) surface saturated with atomic hydrogen generated from a hot rhenium filament (>10,000 Langmuir H_2).

$$-d\theta/dt = \text{desorption rate}(DR) = v_d\theta^n \exp(-E_d/RT)$$

where

θ, surface coverage;
v_d, desorption jump frequency/pre-exponential;
n, rate order;
E_d, desorption activation energy.

In principal, v_d, n, and E_d can all be dependent on θ; however, most analyses assume these parameters to be independent of θ. Using the latter approach and taking the logarithm of both sides of the above equation accompanied by mathematical rearrangement, one obtains:

$$\ln(DR) - n\ln\theta = \ln v_d - E_d/RT$$

If the correct rate order (n) is chosen, a plot of $(\ln(DR) - n\ln\theta)$ vs. $(1/T)$ yields a straight line and has a slope of $-E_d/R$ and a y-intercept of $\ln v_d$. The mathematical methods used for analyzing $(\ln(DR) - n\ln\theta)$ vs. $(1/T)$ were identical to those of Parker et al. [129]. Once n, v, and E_d were determined from the above analysis, fits to the experimental data were generated by simply plotting $d\theta/dt$ using the Polanyi–Wigner equation and the extracted kinetic parameters.

XPS spectra were collected using Al Kα radiation ($h\nu$ = 1486.6 eV) and a 100 mm hemispherical electron energy analyzer (VG CLAM II). AES analysis was performed using a 3 keV, 1 mA beam. Each Auger spectrum was collected in the undifferentiated mode and numerically differentiated. In LEED, an 80 eV, 1 mA beam was used. Oxygen and adventitious carbon levels remained below the detection limits of both XPS and AES during the course of the atomic hydrogen exposure and TPD experiments.

3. Results

Fig. 1 displays a m/e^- = 2 TPD spectrum for hydrogen desorption from a (7 × 7) Si(1 1 1) surface saturated with atomic hydrogen (>10,000 Langmuir). The β_1 and $\beta_{2,3}$ desorption peaks, respectively, attributed to mono and di/trihydride desorption are clearly evident. A $(\ln(DR) - n\ln\theta)$ vs. $(1/T)$ analysis (for the β_1 peak only) clearly indicates second order desorption kinetics with an E_d and v_d of 1.8 ± 0.1 eV and 1 ± 2 × 10^{-5} cm^2/s, respectively. These values are in excellent agreement with those reported by Kleint and Brzoska [66,67] for hydrogen flash desorption experiments from Si surfaces, but are in conflict with the more generally accepted values of E_d = 2.4–2.7 eV and v_d = 0.25–230 cm^2/s [56,68–72]. As noted by Parker et al. [129], analysis and extraction of kinetic parameters from TPD spectra is extremely sensitive to background subtraction and establishing a correct baseline. To test if the above discrepancy was a result of differences in background subtraction, we attempted to account for the possibility of the $\beta_{2,3}$ peak continuing to contribute a relatively constant H_2 desorption rate through the β_1 state by resetting the baseline for the β_1 peak in our (7 × 7) Si(1 1 1) TPD spectra equal to the height of the $\beta_{2,3}$ peak. In this case, a new $(\ln(DR) - n\ln\theta)$ vs. $(1/T)$ analysis yielded a significantly higher E_d and v_d of 2.5 ± 0.2 eV and 2.5 ± 1 cm^2/s for second order kinetics (see Fig. 2). These values are in strong agreement with the now generally accepted values for monohydride desorption from Si(1 1 1) surfaces and highlights the impact of background subtraction in the extraction of kinetic parameters from TPD spectra. It also suggests that the discrepancy between the initial reports of E_d by Klient and Brzoska and later studies could simply be a result of differences in procedures for background subtraction and establishing a baseline.

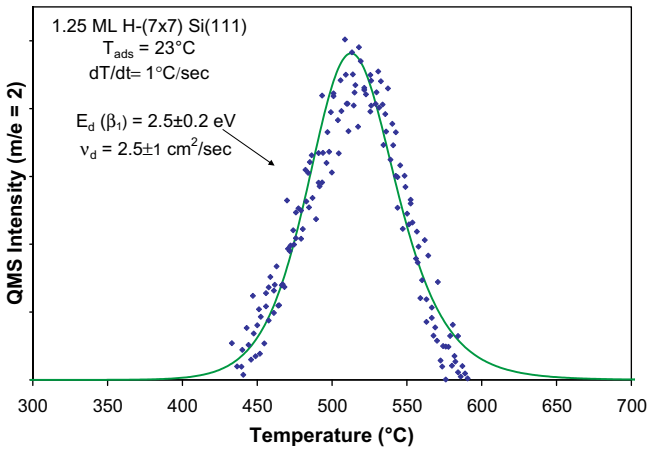

Fig. 2. H_2 (m/e^- = 2) TPD spectrum from a (7 × 7) Si(1 1 1) surface saturated with atomic hydrogen with baseline set equal to the height of the $\beta_{2,3}$ desorption peak. Spectrum illustrates the impact on kinetic parameters determined from TPD spectrum when using an incorrectly established baseline.

Fig. 3a presents a m/e^- = 2 TPD spectrum acquired from a (3 × 3) 6H–SiC (0 0 0 1) surface obtained via annealing and cooling in SiH_4. For this surface, a small desorption peak was observed in the vicinity of 590 °C. Based on the integrated area from our H_2-(7 × 7) Si(1 1 1) TPD spectrum and the results of Culbertson [65], we estimate this hydrogen desorption peak to represent about 0.2 ± 0.05 ML (in SiC(0 0 0 1) units where 1 ML 6H–SiC(0 0 0 1) = 1.2 × 10^{15} atom/cm^2 = 1.5 × 1 ML Si(1 1 1)). The $(\ln(DR) - n\ln\theta)$ vs. $(1/T)$ analysis for the SiH_4-(3 × 3) 6H–SiC(0 0 0 1) surface indicates second order kinetics (see Fig. 4) with an activation energy for desorption E_d of 2.4 ± 0.2 eV. An excellent fit is obtained with these parameters (see Fig. 3). Based on analogy to hydrogen desorption from Si surfaces, we label this the β_1 peak. Post TPD, the (3 × 3) LEED pattern was observed to persist and no changes in surface composition were observed using XPS or AES.

Also included in Fig. 3 is a TPD spectrum from a (3 × 3) 6H–SiC(0 0 0 1) surface prepared via annealing and cooling in SiH_4 and then exposed at room temperature to atomic hydrogen generated from a hot rhenium filament (3000 Langmuir). The atomic hydrogen exposure was observed to produce significant changes in the TPD spectrum from the SiC(0 0 0 1) surface. Most notable was the appearance of a broad H_2 desorption peak that started to develop at temperatures as low as 200 °C and peaked at ~370 °C.

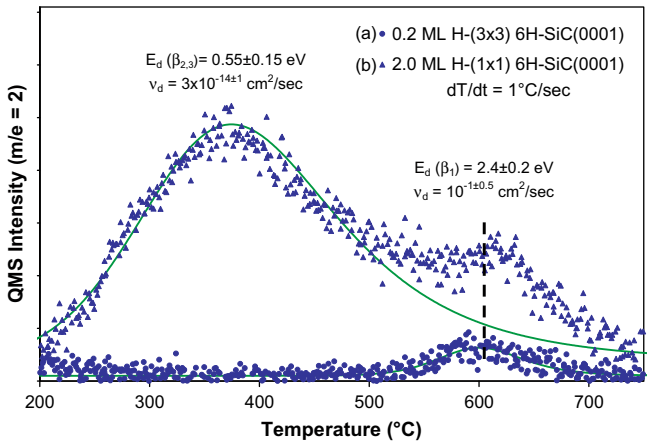

Fig. 3. H_2 TPD spectrum from (a) (3 × 3) 6H–SiC(0 0 0 1) surface prepared by annealing and cooling in SiH_4 (b) SiH_4-(3 × 3) 6H–SiC(0 0 0 1) surface exposed to atomic hydrogen generated by a hot rhenium filament (3000 Langmuir H_2).

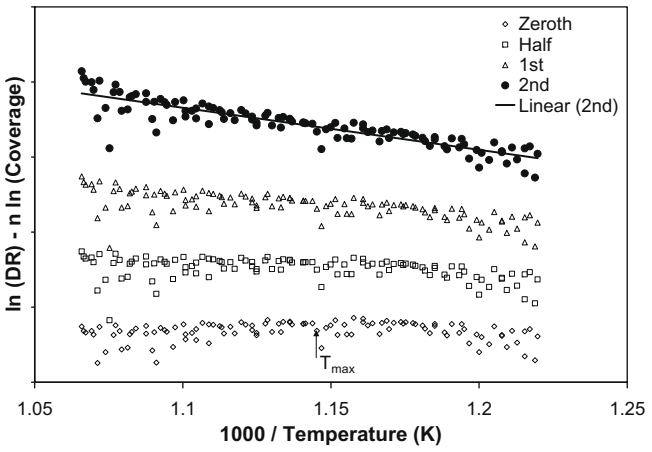

Fig. 4. $\ln(DR) - n\ln\theta$ vs. $1/T$ analysis for β_1 H_2 desorption peak from a SiH_4-(3×3) 6H–SiC(0 0 0 1) surface.

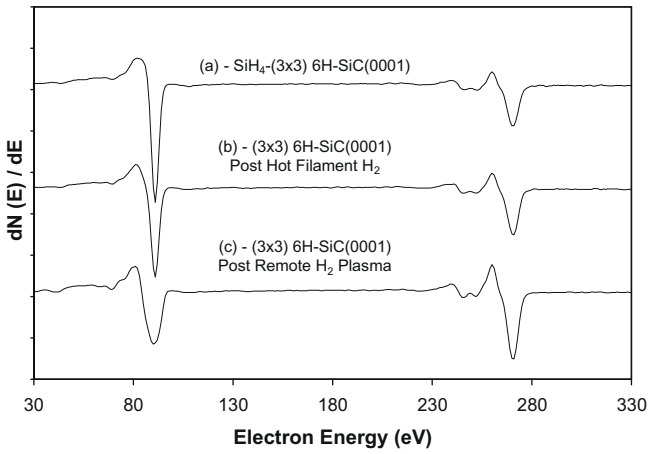

Fig. 6. AES spectra from 6H–SiC(0 0 0) surfaces after (a) annealing and cooling in SiH_4 to produce a (3×3) surface, (b) exposing a (3×3) 6H–SiC(0 0 0 1) surface to atomic hydrogen generated from a hot rhenium filament (3000 Langmuir H_2), and (c) exposing a (3×3) surface to a 5 min 400 °C remote H_2 Plasma.

By analogy to H_2–Si desorption, we label this peak the $\beta_{2,3}$ peak. The integrated area for this peak was indicative of as much as 1.4–2.4 ML of H_2 desorbing from this SiC surface. A $(\ln(DR) - n\ln\theta)$ vs. $(1/T)$ analysis of this peak (see Fig. 5), indicates second order kinetics but with a very small E_d of 0.55 ± 0.15 eV ($\nu_d = 3\times10^{-14\pm1}$ cm^2/s). Though the $\beta_{2,3}$ peak dominates the TPD spectrum from the atomic H exposed surface, the β_1 peak was still observed in some cases (see Fig. 3b). Similar H_2 TPD spectra were also obtained from (3×3) 6H–SiC(0 0 0 1) surfaces that were ramped to 1200 °C to desorb surface hydrogen prior exposure to hot filament generated atomic hydrogen.

LEED, AES, and XPS analysis of the SiH_4 cooled (3×3) 6H–SiC(0 0 0 1) surface before and after exposure to atomic hydrogen also indicated significant changes to this surface. First, the LEED pattern for the (3×3) surface was observed to weaken in intensity and some in cases to revert back to (1×1) after the atomic hydrogen exposure. Second, both AES and XPS showed a decrease in the Si/C ratio after atomic hydrogen exposure. Using AES and accounting for the 2:1 sensitivity difference for Si to C [130], the Si LVV/C KLL peak–peak height (pph) ratio was observed to decrease from ≈1.35 to 0.9 with atomic hydrogen exposure (see Fig. 6a and b). Likewise, XPS showed a decrease in intensity for the Si2p (data not shown). Post TPD, the LEED pattern was observed to revert back to (3×3) in some cases and in others the (1×1) pattern persisted. The re-appearance of the (3×3) reconstruction depended on the time of exposure with long exposures resulting in an absence of re-appearance for this reconstruction. These results all indicate that room temperature atomic hydrogen exposure significantly changes the structure and chemical composition of the (3×3) 6H SiC(0 0 0 1) surface by etching excess Si from the SiC(0 0 0 1) surface.

For the SiH_4 cooled (3×3) 6H–SiC(0 0 0 1) surface exposed to atomic hydrogen from a remote H_2 plasma, similar but more drastic changes were also observed using LEED, AES, XPS, and TPD. The remote H_2 plasma was observed to convert the LEED pattern from (3×3) to a clear (1×1) symmetry indicating complete removal of the Si over layer on the SiC surface. This was confirmed by both AES and XPS. The AES Si/C pph ratio was observed to decrease from 1.35 to <0.5 with remote H plasma exposure (see Fig. 6c), and XPS likewise showed the complete removal of the Si–Si Si2p peak after remote H_2 plasma exposure (See Fig. 7). Interestingly, the peak positions of both the Si2p and C 1s core levels were also observed by XPS to increase in binding energy by ≈0.5 eV after the remote H_2 plasma exposure (see Fig. 7). This indicates a change in band bending at the SiC surface that will be discussed later.

TPD for the remote H plasma exposed (3×3) 6H–SiC(0 0 0 1) surface showed the same broad $\beta_{2,3}$ desorption peak as the

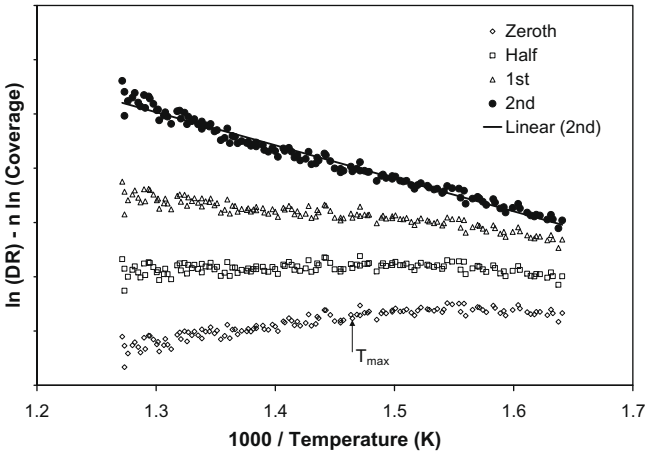

Fig. 5. $\ln(DR) - n\ln\theta$ vs. $1/T$ analysis for $\beta_{2,3}$ H_2 desorption peak from a SiH_4-(3×3) 6H–SiC(0 0 0 1) surface exposed to atomic H generated by a hot rhenium filament (3000 Langmuir H_2).

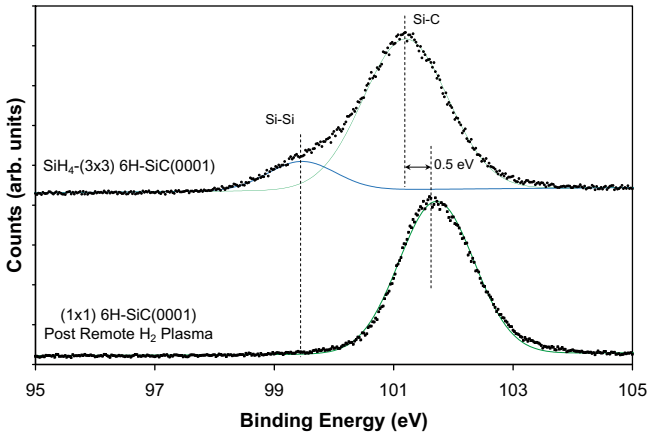

Fig. 7. XPS spectrum from 6H–SiC(0 0 0 1) surface after (a) annealing and cooling in SiH_4 to produce a (3×3) surface, and (b) exposing a (3×3) 6H–SiC(0 0 0 1) surface to a 5 min 450 °C remote H_2 plasma.

(3×3) surface exposed to atomic hydrogen generated via the hot rhenium filament (see Fig. 8). However, the intensity of the $\beta_{2,3}$ peak from the remote H plasma was not nearly as strong and only corresponded to 0.5 ± 0.05 ML. Second order desorption kinetics were still observed, but with a slightly higher desorption activation energy $E_d = 0.7 \pm 0.15$ eV ($\nu_d = 3 \pm 3 \times 10^{-12}$ cm^2/s). No signs of a β_1 silicon monohydride H_2 desorption peak were observed from this surface.

One new feature which consistently appeared in the TPD spectra for the remote H plasma exposed 6H–SiC(0 0 0 1) surfaces was a second higher temperature desorption peak in the range of 650–850 °C (see Fig. 9). In some cases, this desorption peak was clearly resolved into two peaks which we label α_1 and α_2. The integrated area for this peak doublet indicated that this desorption feature corresponded to 0.25 ± 0.05 ML. The $(\ln(DR) - n \ln \theta)$ vs. $(1/T)$ analysis for the α_1 peak indicated second order kinetics (see Fig. 10) with a desorption activation energy E_d of 4.15 ± 0.15 eV ($\nu_d = 2 \times 10^{5\pm1}$ cm^2/s). A slightly higher desorption activation energy E_d of 4.35 ± 0.15 eV ($\nu_d = 2 \times 10^{5\pm1}$ cm^2/s) was also estimated by a similar $(\ln(DR) - n \ln \theta)$ vs. $(1/T)$ analysis. As shown in Fig. 9, an excellent fit of the spectra is obtained with these parameters.

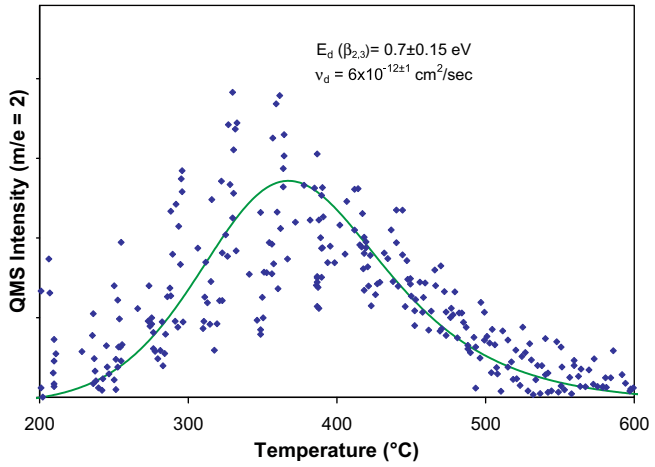

Fig. 8. H_2 ($m/e^- = 2$) TPD spectrum from a (3×3) 6H–SiC(0 0 0 1) surface exposed to a 5 min 450 °C remote H_2 plasma. Spectrum illustrates the low temperature $\beta_{2,3}$ H_2 desorption peaks observed from this surface.

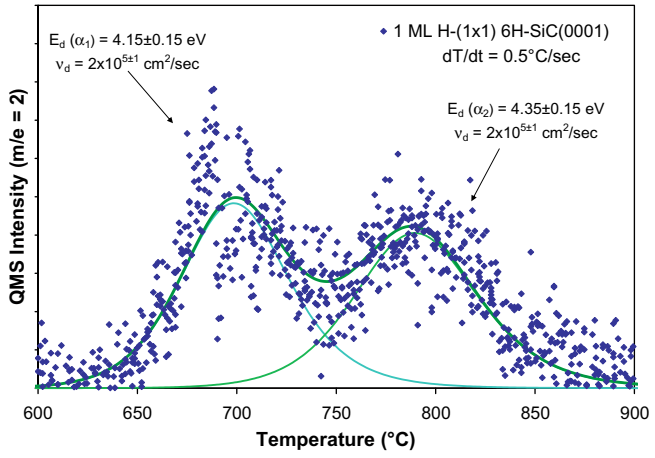

Fig. 9. H_2 ($m/e^- = 2$) TPD spectrum from a (3×3) 6H–SiC(0 0 0 1) surface exposed to a 5 min 450 °C remote H_2 plasma. Spectrum illustrates the higher temperature α_1 and α_2 H_2 desorption peaks observed from this surface.

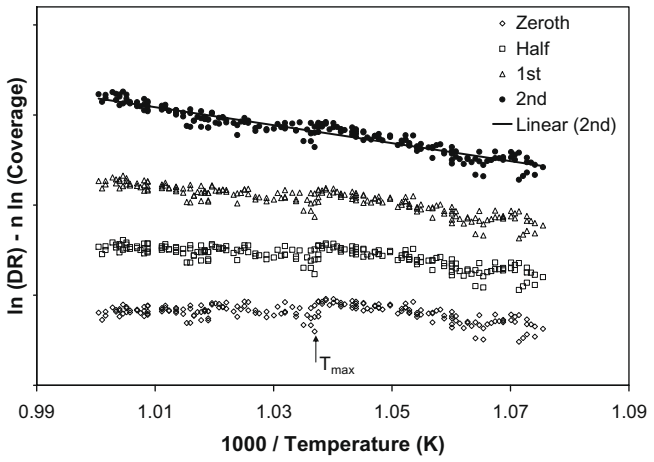

Fig. 10. $\ln(DR) - n \ln \theta$ vs. $1/T$ analysis for α_1 H_2 desorption peak from a (3×3) 6H–SiC(0 0 0 1) surface exposed to a 450 °C remote H_2 plasma.

The LEED pattern for the (3×3) 6H–SiC(0 0 0 1) surface exposed to the remote H_2 plasma remained (1×1), and no change was observed in the Si/C pph ratio in AES studies. The XPS peak positions for the Si2p and C1s core levels did not change after hydrogen thermal desorption. However, a small tail at higher binding energy was observed to develop on the C1s peak which suggests the possible formation of some C–C bonding at the SiC surface after H_2 desorption from the remote H_2 plasma exposed surface, as shown in Fig. 11.

To rule out that any of the observed H_2 desorption peaks from our remote H_2 plasma treated surfaces were actually due to H_2 desorption from our molybdenum sample holder or tantalum mounting wires, we additionally performed TPD on a 1″ diameter molybdenum mounting plate inserted in place of our SiC wafer. Prior to the remote H_2 plasma, the molybdenum plate was degreased in solvents and outgassed at >1000 °C for 3 h. Fig. 12 shows the TPD spectrum acquired from the 1″ diameter molybdenum mounting plate exposed to the remote H_2 plasma. As can be seen, a very large and broad desorption peak corresponding to >5 ML H_2 desorption was observed from this surface with T_{max} occurring at 660 °C. The second order kinetics and activation energy of 1 ± 0.1 eV determined from the ln *DR* vs. $1/T$ analysis is in agreement with previously reported results for H_2 desorption from Mo surfaces [131–135] (see Table 5). A second TPD spectrum collected after the molybdenum plate cooled to room temperature

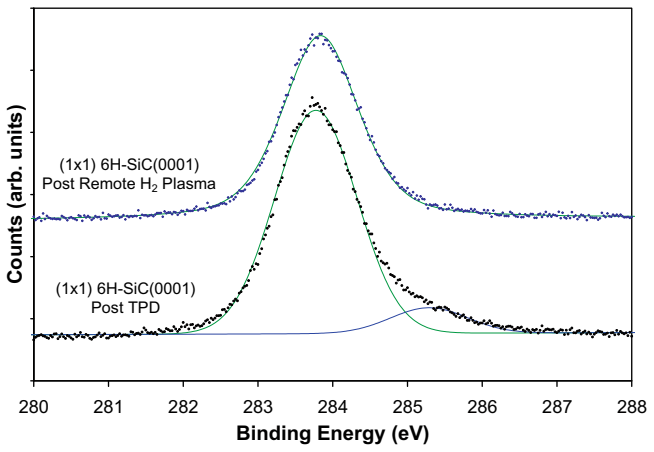

Fig. 11. Pre and post TPD C1s XPS spectrum from a (3×3) 6H–SiC(0 0 0 1) surface exposed to a 450 °C remote H_2 plasma.

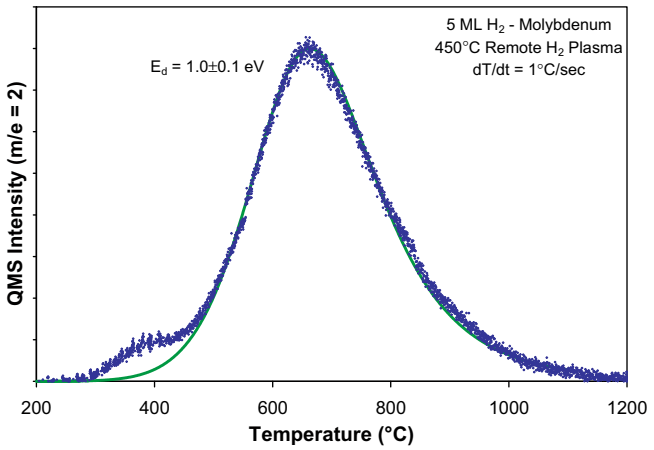

Fig. 12. H_2 ($m/e^- = 2$) TPD spectrum from a 1″ molybdenum mounting plate prepared by solvent decreasing and annealing in vacuum at >1000 °C followed by a 2 min. 450 °C remote H_2 plasma.

was essentially flat up to >850 °C. Based on these results, we believe that H_2 desorption from our sample holder certainly does contribute to a linear background, but does not contribute to any of the key peaks observed in our H_2 TPD spectra.

4. Discussion

4.1. SiH_4-(3 × 3) 6H–SiC(0 0 0 1)

To the authors knowledge, there are no prior reports for the desorption kinetics of hydrogen from single crystalline SiC surfaces. For this reason, we will initially compare our H_2 desorption kinetics from the various 6H–SiC(0 0 0 1) surfaces to those from other crystalline surfaces on which similar Si–H and C–H chemical bonds can be formed (e.g. Si(1 1 1) and C(1 1 1)). Comparison to H–Si(1 1 1) surfaces is particularly justified for H_2 desorption from the (3 × 3) 6H–SiC(0 0 0 1) surface which has been conclusively shown to consist of a full Si–Si bilayer overlaying the bulk SiC crystal surface [125]. In this regard, our observation of second order desorption kinetics and $E_d = 2.4 \pm 0.2$ eV for β_1-H_2 desorption from (3 × 3) 6H–SiC(0 0 0 1) prepared via annealing and cooling in SiH_4 is clearly consistent with the reports of second order kinetics and $E_d = 2.4$–2.7 eV for H_2 desorption from monohydride species on Si(1 1 1) surfaces [68–71]. Due to these similarities, we attribute the β_1-H_2 desorption peak from SiH_4-(3 × 3) 6H–SiC(0 0 0 1) to desorption of H_2 from monohydride Si–H species terminating the Si–Si bilayer on the SiC(0 0 0 1) surface. This assignment is further supported by the observation of 0.2 ± 0.05 ML of H_2 desorbing from the β_1 peak on the (3 × 3) surface. The detailed structure of the (3 × 3) surface has been determined to consist of a planar ad layer of eight silicon atoms topped with a tetrahedral Si ad cluster that produces only one Si dangling bond per (3 × 3) unit cell [136,137]. If that dangling bond was terminated by hydrogen, it would represent ≈0.13 ML of hydrogen on the surface. As our (3 × 3) 6H–SiC(0 0 0 1) surfaces were prepared by annealing and cooling in SiH_4 to below the β_1 desorption state, it is reasonable to expect many of the silicon dangling bonds to be terminated by hydrogen. In fact, Gates et al. [138,139] have shown using TPD and static secondary ion mass spectroscopy (SSIMS) that SiH_4 exposures on the order of $5 \times 10^{20}/cm^2$ is sufficient to saturate all dangling bonds on the (7 × 7) Si(1 1 1) surface. Thus, the observation of 0.2 ± 0.05 ML H_2 desorption from the β_1 peak is consistent with the amount of hydrogen expected to be present on the surface based on the number of available dangling bonds on the (3 × 3) surface that could be terminated by hydrogen. The low H_2 surface coverage on the (3 × 3) 6H–SiC(0 0 0 1) is also responsible for the higher T_{max} for H_2 desorption relative to that observed for (7 × 7) Si(1 1 1). Due to the second order kinetics, T_{max} is a function of coverage and for the (3 × 3) 6H–SiC(0 0 0 1) surface H_2 T_{max} would decrease with increasing coverage approaching the value observed for Si(1 1 1).

4.2. (3 × 3) 6H–SiC(0 0 0 1) post thermal atomic H

Exposing the (3 × 3) 6H–SiC surface to various forms of atomic hydrogen significantly changed the observed TPD spectrum. With small atomic hydrogen exposures generated by cracking H_2 over a hot rhenium filament, the (3 × 3) LEED pattern weakened and a broad H_2 desorption peak ($\beta_{2,3}$) appeared at a temperature well below the β_1 desorption peak. With large atomic hydrogen exposures (e.g. remote H_2 plasma), the (3 × 3) LEED pattern and β_1 peak disappeared all together and a higher temperature H_2 desorption peak ($\alpha_{1,2}$) appeared at 650–850 °C. Our XPS and AES results indicate that these changes in LEED and TPD are due to a change in surface composition/termination brought about by atomic hydrogen etching of the excess Si that produces the (3 × 3) reconstructed surface. Atomic hydrogen induced restructuring and etching of the (3 × 3) 6H–SiC surface has been previously reported by other authors [45–48,50]. In particular, the LEED study by van Elsbergen et al. [45] similarly showed that exposing a (3 × 3) 6H–SiC(0 0 0 1) surface to atomic hydrogen (generated by a hot tungsten filament and 3000 Langmuir H_2) induced the LEED pattern to convert to (1 × 1). In that study, the authors noted that annealing at 800 °C desorbed the adsorbed hydrogen and restored the (3 × 3) pattern. However in a separate study by Stoldt et al. [50], the (1 × 1) LEED pattern induced from a (3 × 3) surface by atomic deuterium exposure was observed to persist after annealing at 823 °C when a sufficiently large atomic deuterium dose was used. Both of these results are consistent with our observations. Stoldt et al. have also similarly observed a reduction in the AES Si/C pph ratio for the (3 × 3) 6H–SiC(0 0 0 1) surface when exposed at room temperature to

Table 5
Reported activation energies and pre-exponentials for hydrogen desorption from various molybdenum and tantalum surfaces.

Orientation	Specie	Coverage (ML)	Order	E_d (eV)	ν_d (ν_2 cm^2/s) (ν_1 s^{-1})	Method	Ref.
Mo(1 0 0)	H_2	2	Second	0.5	10^{-7}	Isobar	[133]
Mo(1 0 0)	H_2	1	NS	0.9	10^{-2}	Isobar	[133]
Mo(1 0 0)	H_2	0.5	NS	1.2	10^{-1}	Isobar	[134]
Mo(1 0 0)	H_2	0.23	Second	1.2 ± 0.09	5×10^{-2}	TPD	[131]
Mo(1 0 0)	H_2	1	Second	0.9 ± 0.09	5×10^{-2}	TPD	[131]
Mo(1 0 0)	H_2	2	First	0.7 ± 0.09	10^{13}	TPD	[131]
Mo(211)	H_2	Low	NS	1	NS	Isobar	[134]
Mo(211)	H_2	High	NS	0.7	NS	Isobar	[134]
Ta-Poly	H_2	8	Second	1.3 ± 0.1	NS	TPD	[135]

Isobar = adsorption isobars.

atomic deuterium. Atomic hydrogen etching of Si(1 1 1) and polycrystalline 3C–SiC surfaces at room temperature has also been observed by other authors [9,51,140].

The HREELS results of Stoldt et al. [50] are also particularly germane to understanding the atomic hydrogen induced changes in our (3 × 3) 6H–SiC(0 0 0 1) TPD spectra. For (3 × 3) surfaces exposed at room temperature to sufficiently large atomic deuterium exposures, the HREELS results of Stoldt show the appearance of both Si–D and C–D stretching modes after the (3 × 3) pattern converts to (1 × 1). These experiments indicate that for the (3 × 3) surfaces exposed to thermally generated atomic hydrogen in the present study, there is the possibility for hydrogen to be bonded to both Si and C atoms at the SiC surface. In turn, separate peaks in TPD spectra should be expected due to hydrogen desorbing from both Si–H and C–H surface sites. The occurrence of these processes is supported by the differences in peak temperatures for hydrogen desorption from Si(1 1 1) and C(1 1 1) surfaces which have been reported to be in the approximate ranges of 400–500 °C and 800–1000 °C, respectively [66–72,96,99].

We attribute the $\beta_{2,3}$ H_2 desorption peak observed from the (3 × 3) 6H–SiC(0 0 0 1) surface exposed to atomic hydrogen generated by a hot rhenium filament to molecular hydrogen desorption from a mix of silicon di and trihydrides species. This assignment is supported by the observation of a Si/C ratio >1 in AES and the continued presence of a Si–Si Si2p peak in XPS. It is also supported by TPD investigations of Si(1 1 1) and Si(1 0 0) surfaces where di and trihydride desorption is observed to occur at ≈120 and 200 °C, respectively, below the main β_1 peak [56,57]. In our case, the $\beta_{2,3}$ peak (T_{max} = 370 °C) is ≈220 °C below the β_1 peak, which is consistent with the β_1 vs. β_3 offset observed for Si(1 1 1). Based on this observation, it is tempting to attribute most of the H_2 desorption in our $\beta_{2,3}$ H_2 desorption peak to β_3 trihydride desorption. This would be consistent with the observation of silicon etching by atomic hydrogen, as trihydride species are needed to generate the final etch product silane. In fact, it is possible that silicon etch products such as SiH_4, Si_2H_6, are also desorbing from the SiC surface and contributing to the $\beta_{2,3}$ desorption peak. Desorption of such etch products has been observed in TPD spectra of atomic hydrogen etched Si(1 1 1) surfaces, but the intensity of the peaks were 1/40th to 1/10,000th of the detected H_2 desorption [141]. In our case, we did not detect any desorption peaks from this surface when we monitored the principle SiH_4 RGA fragment (m/e^- = 30). However, this does not preclude their presence given the limited sensitivity for our spectrometer in this experiment.

The SiC $\beta_{2,3}$ E_d of 0.55 eV is substantially lower relative to the E_d of 1.9–2.0 eV reported for β_2 dihydride desorption from Si(1 1 1), Si(1 0 0) and porous Si surfaces [56,71–73,83]. Although no activation energies for β_3 H_2 desorption from Si(1 1 1) or (1 0 0) surfaces have been reported, an activation energy of 1.35 eV has been reported by Greenlief for SiH_4 desorption from Si(1 1 1) surfaces saturated with hydrogen [84]. This E_d is still almost 2× the value we have observed from SiC for $\beta_{2,3}$ desorption. Keroack et al. have reported an E_d of 0.7 ± 0.3 eV for desorption of implanted H_2 from poly-crystalline α-SiC surfaces [120]. However, the temperatures at which the implanted H_2 desorbed was almost 1000 °C higher then our $\beta_{2,3}$ peak.

The low $\beta_{2,3}$ E_d could be a result of the presence of Si–C back bonds, which due to the higher electronegativity of carbon, pulls electrons from the silicon surface atom and thus weakens the Si–H bonding. This behavior has been previously reported for Si(1 0 0) surfaces dosed with either C, Ge, B, or P (see Tables 6 and 7) [142–146]. For the case of carbon, TPD spectra from Si(1 0 0) surfaces dosed with CH_3SiH_3 followed by atomic D exposure showed a third D_2 desorption peak at 480 °C in addition to the β_1 and β_2 peaks at 515 and 405 °C, respectively [143]. This third peak labeled γ exhibited second order desorption kinetics (E_d = 2.22 eV) and was attributed to D_2 desorption from silicon monodueteride surface species where the Si surface atom was back bonded to carbon [143]. Similarly for boron dosed Si(1 0 0) surfaces, lower temperature β_1^* and β_2^* desorption states were observed and attributed to H_2 desorption for silicon surface atoms bonded to sub-surface B [142]. In this case, the reduction in E_d for silicon with boron backbonds was also attributed to the larger electronegativity of boron and the resulting charge transfer away from silicon weakening the Si–H surface bonds. Similar behavior has also been reported for Ge on Si, Si on Ge, [147–152,145]. However, in all these examples, the magnitude of the decrease in E_d is only 0.3–0.4 eV vs. the 0.8–1 eV decrease we have observed. This is very likely a result of the fact that for the C, B, Ge on Si(1 0 0) examples, not all Si atoms are back bonded to the dopant atom and at

Table 6
Reported activation energies and pre-exponentials for hydrogen desorption from various germanium surfaces.

Orientation	Specie	Coverage (ML)	Order	E_d (eV)	ν_d (ν_2 cm^2/s) (ν_1 s^{-1})	Method	Ref.
Ge(0 0 1)	H_2	NS	First	1.7 ± 0.09	1.6×10^{13}	IsoRef	[147]
Ge(1 1 1)	H_2	0–1	Second	1.5 ± 0.1	NS	TPD	[148]
Ge(0 0 1)	H_2	NS	First	1.7 ± 0.1	$2 \pm 1 \times 10^{13}$	SDR	[149]
(2 × 1) Ge(0 0 1)	H_2	0–1	First	1.8	NS	TPD	[150]
(2 × 1) Ge(0 0 1)	H_2	0–1	First	1.7 ± 0.1	$4 \pm 1 \times 10^{13}$	LID-TPD	[151]
(2 × 1) Ge(0 0 1)	H_2	0–1	First	1.65 ± 0.1	$2.7 \pm 0.5 \times 10^{13}$	TPD	[152]
(2 × 1) Ge(0 0 1)	D_2	0–1	First	1.65 ± 0.1	$1.2 \pm 0.5 \times 10^{13}$	TPD	[152]
Ge/Si(1 0 0)	H_2	1.5	First	1.7 ± 0.1	2×10^{15}	TPD	[145]

IsoRef = isothermal time resolved reflectometry, LID = laser induced desorption.

Table 7
Reported activation energies and pre-exponentials for hydrogen desorption from various Si(1 0 0) surfaces doped with germanium or boron.

Substrate	Specie	Coverage (ML)	Order	E_d (eV)	ν_d (ν_2 cm^2/s) (ν_1 s^{-1})	Method	Ref.
Si(0 0 1)	β_1-D_2	1.25	First	2.52	1×10^{15}	TPD	[142]
Si(0 0 1)	β_2-D_2	1.25	First	1.88	1×10^{13}	TPD	[142]
B–Si(0 0 1)	β_1-D_2	0.75	First	2.29	3×10^{14}	TPD	[142]
B–Si(0 0 1)	β_2-D_2	0.75	First	1.56	1×10^{12}	TPD	[142]
C–Si(0 0 1)	γ-D_2	1.0	Second	2.22	1×10^{14}	TPD	[143]
Si(0 0 1)-10% Ge	D_2	0–1.5	First	2.33	2×10^{15}	TPD	[144]
Si(0 0 1) (0–1ML Ge)	H_2	0–1.5	First	$2.52 - 0.32\theta_{Ge}$	1×10^{15}	TPD	[145]
Ge(0 0 1) (0–1ML Si)	H_2	0–1.5	First	$1.8 + 0.15\theta_{Si}$	5×10^{14}	TPD	[145]

most only two Si-dopant back bonds can be formed. For our case, it much more likely that the Si surface atom is back bonded to up to three carbon atoms due to working with a (0 0 0 1) single crystalline surface. Alternatively, the low $\beta_{2,3}$ E_d could simply represent the inherent instability of the hydrogenated Si–Si bilayer on the SiC surface or H_2 desorption from numerous different di/trihydride sites all with slightly different desorption kinetics that we are unable to resolve in our TPD measurements.

Considering the coverage of 1.4–2.4 ML H_2 desorption determined for the $\beta_{2,3}$ peak, we note that these results are in agreement with the time-of-flight elastic recoil detection analysis (TOF-ERDA) measurements by Fujino et al. [46]. Their TOF-ERDA measurements determined that exposing a ($\sqrt{3} \times \sqrt{3}$) 6H–SiC(0 0 0 1) surface to a saturation exposure of hot filament generated atomic hydrogen results in the adsorption of 1.7 ML of hydrogen on this surface. Although the ($\sqrt{3} \times \sqrt{3}$) reconstructed surface is not the same as our (3 × 3) surface, their coaxial impact-collision ion scattering spectroscopy (CAICISS) measurements indicate this reconstruction consists of a Si adatom on a T_4 site. In a separate study, we have also generated ($\sqrt{3} \times \sqrt{3}$) reconstructed 6H–SiC surfaces by simply annealing our (3 × 3) surface in vacuum and desorbing excess Si and have found these surfaces still have an AES Si/C pph ratio of ≈1.1 [125]. The Fujino ($\sqrt{3} \times \sqrt{3}$) surface, therefore represents a SiC(0 0 0 1) surface with excess Si and probably a similar number of dangling bonds to saturate as for our atomic hydrogen etched (3 × 3) surfaces. Therefore, our observation of 1.4–2.4 ML of H_2 desorption from the $\beta_{2,3}$ state is consistent with the results of Fujino, which serve as an additional reference/calibration point for our H_2 TPD measurements from 6H–SiC(0 0 0 1) surfaces.

4.3. (3 × 3) 6H–SiC(0 0 0 1) post remote H_2 plasma

For the TPD spectra acquired from a (3 × 3) 6H–SiC(0 0 0 1) surface exposed to a remote H_2 plasma, we obtained a slightly higher E_d of 0.7 ± 0.15 eV for the $\beta_{2,3}$ peak. Due to the change in Si/C surface stoichiometry from 1.35 to <0.5 with the remote H_2 exposure, this change in E_d could be attributed to a change in hydrogen desorbing from predominantly $SiH_{2,3}$ species to $SiH_{2,3}$ and/or $CH_{2,3}$ sites. Such an assignment would be supported by the HREELS results of Stoldt et al. where both Si–D and C–D stretches were observed on the SiC(0 0 0 1) surface after the (3 × 3) reconstruction had been converted to (1 × 1) by a long atomic deuterium exposure. In this regard, it is interesting to note that in several studies the value of E_d reported for H_2 desorption from graphite falls in the range of 0.7–1.2 eV [87,107,110,111]. Though these values are in agreement with our $\beta_{2,3}$ E_d, the temperatures at which H_2 desorption from graphite were detected and at which E_d was determined are substantially higher at 600–1000 °C. Thus, it is unlikely the two are related.

It is possible that the broad desorption peak for the remote H_2 plasma exposed SiC(0 0 0 1) surface is due to the roughening of the SiC surface on an atomic scale by the remote H_2 plasma. Atomic scale roughening and broadening of H_2 desorption peaks has also been observed for C(1 0 0) and C(1 1 1) surfaces exposed to thermal and/or plasma atomic hydrogen sources [95,96,103]. In this regard, Kim and Olander were able to detect SiH_4 and CH_4 production in their atomic hydrogen modulated molecular beam mass spectrometry (MMBMS) studies on poly-crystalline 3C–SiC samples that also revealed preferential attack at grain boundaries [52]. However, the deduced activation energies of 0.03–0.06 eV are incredibly lower then our $\beta_{2,3}$ E_d. Thus, we are left with attributing the $\beta_{2,3}$ state to hydrogen desorption from remaining silicon di/trihydride species.

Concerning the $\alpha_{1,2}$ desorption peaks observed from the (3 × 3) 6H–SiC(1000) surfaces exposed to a remote H_2 plasma, we assign this desorption state to hydrogen desorption from carbon surface sites. This assignment is supported by the post remote H_2 plasma AES Si/C ratio of <1 that indicates a carbon rich surface, and the post TPD XPS C1s data showing the formation of some C–C bonding at the surface (presumably to eliminate dangling bonds generated by the liberation of hydrogen from the surface). The presence of some C–H species is also to be expected based on the HREELS measurements of Stoldt, as previously discussed. Further, H_2 and D_2 desorption from carbon monohydrides present on Si(1 0 0) surfaces (from adsorbed C_2H_2 or CH_3SiH_3) has been observed to occur at 650–870 °C [143,153]. This is consistent with the temperature range for our $\alpha_{1,2}$ desorption peaks. Unfortunately, neither study reported desorption activation energies for these states.

Additional support for this assignment is provided by comparison of the E_d determined for our $\alpha_{1,2}$ peak with those determined for H_2 and D_2 desorption from C(1 1 1) surfaces which range from 2.9–4.0 eV [96–99]. Although this is a large spread in E_d, the majority of the values fall in the range of 3.5–4.0 eV for C(1 1 1). Our SiC(0 0 0 1) $\alpha_{1,2}$ E_d values of 4.15 and 4.35 ± 0.15 eV although on the high end are clearly inline with the D-C(1 1 1) values. It should be emphasized that the above E_d values for C(1 1 1) are primarily for D_2 desorption, and those reported here for 6H–SiC(0 0 0 1) are for H_2 desorption. While kinetic isotope effects have been shown to result in different pre-exponentials for H_2 and D_2 desorption, this effect does not generally cause the desorption order or activation energies to differ. Lastly, it is interesting to note that the predominance of E_d values reported for both H_2 and D_2 desorption from C(1 0 0) surfaces are similar to those for C(1 1 1) surfaces but slightly lower at 3.15–3.5 eV. This is analogous to the case for H_2 desorption from Si(1 1 1) and Si(1 0 0) surfaces, where the E_d for Si(0 0 1) is slightly lower relative to Si(1 1 1).

Although the activation energy for our $\alpha_{1,2}$ desorption states are close to those reported for H_2 desorption from C(1 1 1) surfaces, the desorption kinetics are completely different with second order kinetics being observed from our SiC surfaces and first order kinetics for H_2 desorption from C(1 1 1). In this regard, our observation of second order kinetics are more consistent with H_2 desorption from Si(1 1 1) where second order kinetics are also observed. The differences in hydrogen desorption order kinetics between C(1 1 1) and Si(1 1 1) have been previously noted and attributed to a number of different mechanisms for the C(1 1 1) surface including defect sites, delocalized band states, pre-pairing and domain formation mechanisms [98]. The exact mechanism for H_2 desorption from C(1 1 1) surfaces still remains to be determined. However, the observation of second order H_2 desorption kinetics from the 6H–SiC(0 0 0 1) surface suggests it may be more similar to the mechanism for second order H_2 desorption from Si(1 1 1).

One additional difference between H_2 desorption from carbon rich 6H–SiC(0 0 0 1) surfaces and C(1 1 1) surfaces is that the observed T_{max} for H_2 desorption from C(1 1 1) and C(1 0 0) surfaces is substantially higher then that observed for our $\alpha_{1,2}$ H_2 desorption peak from 6H–SiC(0 0 0 1) (650–850 vs. 800–1000 °C). This difference can be partly explained by the differences in heating rates used in the diamond TPD experiments vs. ours. In the diamond TPD experiments, heating rates as high 35–40 °C/s were used vs. the heating rates of 0.5–1 °C/s used in our experiments. For second order desorption kinetics, T_{max} is a function of the heating rate. Using the kinetics determined for α_1 and changing the heating rate to 40 °C/s, we determine that T_{max} would increase by ≈100 °C which would put our T_{max} much closer to that observed from diamond.

As for other studies of H_2 desorption from SiC surfaces, the only relevant reports of which the authors are aware are those by Sieber et al. [33] and Allendorf and Outka [51]. In the Sieber study, FTIR-ATR was used to monitor the surface Si–H stretch intensity as a function of temperature for a hydrogen terminated (0 0 0 1) 6H–SiC surface prepared by annealing in flowing H_2 at 1000 °C. This preparation technique generates a (1 × 1) surface terminated with

1 ML of Si–H bonds. Their FTIR-ATR results show that with annealing at increasing temperatures a gradual decline in Si–H coverage starts at ~550–600 °C with a steep drop to zero in Si–H intensity occurring at 775 °C. On completion of H_2 desorption at this temperature, the 6H–SiC surface converts from (1×1) into a $(\sqrt{3} \times \sqrt{3})$ reconstruction which based on XPS measurements, Sieber attributes to a Si rich adatom structure. Unfortunately, it is difficult to compare these results to any of our TPD results due to the large differences in preparation methods and surface stoichiometry. The most relevant comparison between our results and those of Sieber would be our TPD results from SiH_4-(3×3) 6H–SiC(0 0 0 1). In this case, H_2 desorption from the SiH_4-(3×3) surface is observed to peak at 590 °C and return to baseline by ~715 °C. The latter temperature is slightly lower than the temperature of 770 °C shown in the Sieber study. This difference, however, could easily be the result of differences in heating rates and H_2 pumping speeds between the two studies.

The other relevant study to which our results can be compared is that by Allendorf and Outka [51]. In that study, H_2 TPD was performed on poly-crystalline 3C–SiC samples exposed to thermally generated atomic hydrogen. Ar ion sputtering and flash annealing to 1123 °C was used to remove oxygen from the as loaded SiC surface and the resulting AES Si/C ratio was 0.54–0.67. For surfaces prepared in this fashion and then exposed to thermally generated atomic hydrogen, they observed the AES Si/C ratio for these surfaces to decrease further to 0.46 indicating silicon etching by the atomic hydrogen exposure and agreement with our results. The H_2 TPD spectra from their surfaces showed H_2 desorbing in a broad peak ranging from 423 to 1000 °C. They resolved this broad peak into two desorption states with peaks at 703 and 857 °C. The TPD spectra from this surface are most comparable to our TPD spectra from (3×3) 6H–SiC(0 0 0 1) surfaces exposed to a remote H_2 plasma. In this case, the positions of our α_1 and α_2 peaks at 700 and 790 °C are in particularly close agreement to those reported by Allendorf and Outka. If one factors in the faster heating rate of 4.9 °C/s used by Allendorf and Outka vs. the 0.5 °C/s used in our experiments, one would expect our $\alpha_{1,2}$ peaks to increase in temperature by ~50 °C and move into closer agreement. However, Allendorf and Outka assumed first order desorption kinetics and determined significantly lower activation energies for H_2 desorption of 2.7 and 3.1 eV, respectively. In our case, we determined second order desorption kinetics with much higher E_d. If we assumed first order desorption kinetics in our ln (DR) vs. $1/T$ analysis, we would obtain E_d of 2.6 and 2.9 eV for our α_1 and α_2 peaks, respectively. These values are in much closer agreement with those of Allendorf and Outka and indicate that the difference in E_d values is simply a result of the assumption of first order kinetics by Allendorf and Outka. It should be again noted that the samples used in the Allendorf and Outka study were poly-crystalline and in the MMBMS studies by Kim and Olander [52] on similar samples, preferential attack of the grain boundaries by atomic hydrogen was observed. In order to account for this large surface heterogeneity, Allendorf and Outka fit their H_2 TPD spectrum assuming a Gaussian distribution of multiple desorption sites with an average cumulative activation energy equal to the values reported. Therefore, the derived agreement between their results and those in this study might be somewhat serendipitous.

It is also interesting to note that H_2 desorption activation energies of 3.7–4.0 eV have been reported for poly-crystalline and α-SiC samples implanted with high energy H^+/H_2^+ ions [118,121]. In these cases, H_2 desorption from these surfaces is observed to occur at >800 °C and is attributed to sub-surface H trapped at carbon sites. Although not directly applicable, these results are in qualitative agreement with our TPD study.

Some discussion regarding the origin of the $\alpha_{1,2}$ peak doublet is merited. Based on analogy to the Si(1 1 1) surface, it is tempting to attribute this peak doublet to H_2 desorption from carbon monohydride and dihydride surface species. Another possibility is that both are due to carbon monohydride desorption. Flowers et al. have previously resolved the (7×7) Si(1 1 1) β_1 peak into a doublet that they attributed to H_2 desorption from two geometrically different silicon monohydride surface sites in the (7×7) reconstruction [71]. Due to our use of off-axis wafers, it is possible that such geometry differences could be created by surface steps. It is also possible, that the peak doublet is an artifact of H_2 desorption from the sample holder. In the graphite H_2 TPD studies by Gould [87], a peak doublet was observed in the range of 250–850 °C. The higher temperature H_2 desorption peak centered at 650 °C was attributed to H_2 desorption from the molybdenum sample holder. In our case, we separately monitored H_2 desorption from a molybdenum mounting plate exposed to the remote H_2 plasma and also observed a peak in H_2 desorption at 650 °C (see Fig. 12). As our α_1 desorption state has $T_{max} \cong 700$ °C, it is possible that this peak could be an artifact created by H_2 desorption from our sample holder. However, we determined an E_d of 1.0 eV for the molybdenum H_2 desorption peak and this does not match with the E_d determined for α_1 of 4.15 eV. Detection of spurious H_2 desorption from our Ta mounting wires is also a possibility. In this case, we note that Shleifman et al. [135] have previously examined the desorption of H_2 from poly-crystalline Ta surfaces and noted that H_2 desorbs at ~500 °C, which does not coincide with our $\beta_{2,3}$ or $\alpha_{1,2}$ peaks. We therefore do not think the $\alpha_{1,2}$ doublet is an artifact. Unfortunately based on the data at hand, it is not possible to make any definitive conclusions regarding whether the $\alpha_{1,2}$ peak doublet represents C–H_2 and C–H desorption or H_2 desorption from different C–H sites.

4.4. Atomic H etching of (3×3)–(0 0 0 1) 6H–SiC surfaces

The data in the previous sections clearly illustrate that atomic hydrogen etches excess silicon present on 6H–SiC(0 0 0 1) surfaces. As mentioned previously, these results are consistent with prior investigations of atomic hydrogen etching of Si(1 1 1) [9,51] and (3×3) 6H–SiC(0 0 0 1) surfaces [45,51]. Although the intent of this study was not to investigate the details of the atomic H–Si etch mechanism, our data clearly indicates that at moderately low temperatures (20–450 °C) atomic hydrogen (in sufficient quantities) is capable of removing all excess silicon from 6H–SiC(0 0 0 1) surfaces. Further etching of the outermost Si layer of the 6H–SiC(0 0 0 1) surface may also be possible and is supported by the observation of AES pph ratios of <0.5 for remote H_2 plasma etched surfaces. Additional support is provided by XPS of 6H–SiC(0 0 0 1) surfaces exposed to a remote H_2 plasma and annealed at >1000 °C that shows the formation of graphitic surface. This suggests that exposure of the 6H–SiC(0 0 0 1) surface to atomic hydrogen from the remote H_2 plasma may also be capable of removing the outermost Si layer of the 6H–SiC(0 0 0 1) surface leaving behind a carbon monohydride terminated surface. Based on the data at hand, it is difficult to conclude whether continued etching of the SiC surface occurs beyond removal of the outermost Si layer. However based on the thermal stability of C–H species at temperatures above 450 °C, we postulate that at temperature of <450 °C atomic hydrogen etching of the 6H–SiC(0 0 0 1) surface could stop after removal of the outermost Si layer.

4.5. Band bending at (0 0 0 1) 6H–SiC surfaces

As shown in Fig. 7, the Si2p (and C1s) core levels were observed to shift to 0.5 eV higher binding energy after exposing the (3×3) 6H–SiC(0 0 0 1) surface to the remote H_2 plasma. This result indicates a significant change in band bending at the surface and for our n-type surfaces specifically indicates a downward bending of

the surface bands by 0.5 eV. Valence and conduction band bending at semiconductor surfaces is caused by the introduction of surface states within the bulk forbidden band gap that pins the Fermi level (E_F) at these states. Evidence of surface states and band bending at SiC surfaces has been previously observed for (3×3) 6H–SiC(0 0 0 1) surfaces by several researchers using photoelectron and photoemission spectroscopies and theoretical techniques [155–160]. The photoelectron and photoemission studies have identified three occupied surface states at 0.5, 1.5, and 1.9 eV below E_F [154–158]. The ab initio DFT-LDA calculations by Furthmuller [154] and analogies to the $(\sqrt{3} \times \sqrt{3})$ surface [159,160] indicate that these surface states are likely due to the dangling bond of the Si adatom and the backbonds of the silicon adatom to the Si tetramer in the (3×3) reconstruction. As our Si2p and C1s core levels did not shift after performing H_2 TPD on the freshly prepared SiH_4-(3×3) surface or after exposure and desorption of small doses of thermally generated atomic hydrogen, it is unlikely that the band bending is due to passivating/unpassivating surface dangling bonds. The 0.5 eV shift in Si2p and C1s core levels did not occur until the XPS Si–Si Si2p peak was removed by the remote H_2 plasma exposure. As the Si2p and C1s peak positions remained unchanged after hydrogen desorption, this suggests that for the (3×3) surface, the surface states and band bending are not hydrogen/dangling bond related but silicon adatom related.

Changes in band bending have also been observed for the SiC(1 0 0) surface by Bermudez and Long [161]. Using soft X-ray photoelectron spectroscopy, they observed the binding energy of the SiC(1 0 0) valence band maximum to increase from 1.4 to 2.0 eV as the surface was converted from a Si terminated (2×1) surface to a carbon terminated c(2×2) surface. This result suggests a change in band bending due to silicon related surface states to carbon related surface states. Such a hypothesis is consistent with theoretical calculations for this surface that have indicated the presence of both Si and C dangling bond surface states in the SiC(1 0 0) band gap [162]. The carbon dangling bond surface state is calculated to be lower in energy then the Si dangling bond state and reside close to the valence band maximum.As our observed change in band bending for the 6H–SiC(0 0 0 1) surface also occurs with a change in stoichiometry from silicon rich to carbon rich and is of similar magnitude, the results of Bermudez suggest that Fermi level pinning for out surfaces may also switch from silicon related to carbon related surface states. This observation is consistent with results from the angle resolved photoelectron spectroscopy study by Emtev et al. [158] on hydrogen terminated 6H–SiC(0 0 0 1) and 6H–SiC(0 0 0 $\bar{1}$) surfaces prepared by high temperature annealing in ultra pure H_2. After desorbing the hydrogen termination using undispersed synchrotron radiation, they observed the appearance of surface states at 0.8 and 0.2 eV above the SiC VBM for the (0 0 0 1) and (0 0 0 $\bar{1}$) surfaces respectively. Based on the crystallographic orientation, the (0 0 0 1) and (0 0 0 $\bar{1}$) surface states were, respectively attributed to silicon and carbon dangling bonds. As for the SiC(0 0 1) surfaces, theoretical calculations for the 6H–SiC(0 0 0 1) surface also show the presence of both silicon and carbon dangling bond related surfaces states in the band gap with the carbon dangling bond state residing close to the valence band maximum [160]. However in our case, the change in band banding occurred with exposure to atomic hydrogen from a remote H_2 plasma, and after thermal desorption of the surface hydrogen, no changes in the peak positions for the C1s or Si2p core levels were observed. Thus it is unlikely that the final state of the band bending is Fermi level pinning by carbon dangling bonds. Any additional changes in band bending that might have been observed by creation of carbon dangling bonds via H_2 thermal desorption may have been mitigated by the passivation of those dangling bonds via formation of graphitic surface carbon (as observed). Thus, we conclude that the observed band bending is the result of the elimination of Si adatom surface states and downward band bending to either a flat band condition or Fermi level pinning by some other type of carbon related surface state.

5. Conclusions

The interaction of atomic hydrogen with and the desorption kinetics of molecular hydrogen from various 6H–SiC(0 0 0 1) surfaces were examined using TPD, AES, XPS, and LEED. Depending on the surface stoichiometry, different desorption states were observed in the TPD measurements with second order recombinatory kinetics being determined in most cases. For silicon rich (3×3) 6H–SiC(0 0 0 1) surfaces, H_2 desorption was observed to occur at 590 °C with $E_d = 2.4 \pm 0.2$ and attributed to β_1 silicon monohydride desorption. For (3×3) 6H–SiC(0 0 0 1) surfaces exposed to atomic hydrogen, the LEED pattern was observed to revert to (1×1) and etching of excess silicon from the (3×3) surface was observed by both XPS and AES. XPS additionally showed the Si2p and C1s to increase in binding energy by 0.5 eV. This decrease in surface band bending was attributed to the removal of the Si–Si bilayer that comprises the (3×3) reconstruction. TPD of the hydrogenated $(3 \times 3) \rightarrow (1 \times 1)$ 6H–SiC(0 0 0 1) surfaces showed several additional desorption peaks. A low temperature desorption peak was observed at 370 °C with an E_d of 0.6 ± 0.2 eV and attributed to $\beta_{2,3}$ silicon di/trihydride desorption. Two higher temperature H_2 desorption peaks were also observed at 650–850 °C with E_d of 4.15 and 4.35 ± 15 eV. These peaks were attributed to $\alpha_{1,2}$ H_2 desorption from carbon surface atoms. In conclusion, SiC H_2 desorption kinetics exhibit similarities to both Si(1 1 1) and C(1 1 1) surfaces dependent on the surface stoichiometry.

Acknowledgements

The authors wish to thank Cree, Inc. for the 6H–SiC wafers. The research was supported by the Office of Naval Research under Contract No. N00014-92-J-1477 (M. Yoder, Technical Monitor) and the Department of Education via an Electronic Materials/GAANN Fellowship. R.F. Davis was partially supported by a Kobe Steel, Ltd. Professorship.

References

[1] G.R. Srinivasan, J. Cryst. Growth 70 (1984) 201.
[2] H.S. Kong, J.T. Glass, R.F. Davis, J. Appl. Phys. 64 (1988) 2672.
[3] M. Frenklach, H. Wang, Phys. Rev. B 43 (1991) 1520.
[4] X.C. Mu, S.J. Fonash, G.S. Oehrlein, S.N. Chakravarti, C. Parks, J. Keller, J. Appl. Phys. 59 (1986) 2958.
[5] P.H. Yih, A.J. Steckl, J. Electrochem. Soc. 150 (1993) 1813.
[6] G.S. Higashi, R.S. Becker, Y.J. Chabal, A.J. Becker, Appl. Phys. Lett. 58 (1991) 1656.
[7] G.S. Higashi, Y.J. Chabal, G.W. Trucks, K. Raghavachari, Appl. Phys. Lett. 56 (1990) 656.
[8] S.W. King, R.J. Nemanich, R.F. Davis, J. Electrochem. Soc. 146 (1999) 1910.
[9] R. Carter, T. Schneider, J. Montgomery, R. Nemanich, J. Electrochem. Soc. 141 (1994) 3136.
[10] M.E. Lin, S. Strite, A. Agarwal, A. Salvador, G.L. Zhou, N. Teraguchi, A. Rockett, H. Morkoc, Appl. Phys. Lett. 62 (1993) 702.
[11] O.M. Kuttel, L. Diederich, E. Schaller, O. Carnal, L. Schlapbach, Surf. Sci. 337 (1995) L812.
[12] G.J. Pietsch, Y.J. Chabal, G.S. Higashi, J. Appl. Phys. 78 (1995) 1650.
[13] L. Zhou, V. Audurier, P. Pirouz, J.A. Powell, J. Electrochem. Soc. 144 (1997) L161.
[14] B.B. Pate, Surf. Sci. 165 (1986) 83.
[15] J.P. Sullivan, W.R. Graham, R.T. Tung, F. Schrey, Appl. Phys. Lett. 62 (1993) 2804.
[16] Y.G. Wang, S. Ashok, J. Appl. Phys. 75 (1994) 2447.
[17] T. Tachibana, J.T. Glass, R.J. Nemanich, J. Appl. Phys. 73 (1993) 835.
[18] K. Vanheusden, R.A.B. Devine, Appl. Phys. Lett. 76 (2000) 3109.
[19] K. Fukuda, S. Suzuki, T. Tanaka, K. Arai, Appl. Phys. Lett. 76 (2000) 1585.
[20] S. Dhar, L.C. Feldman, S. Wang, T. Isaacs-Smith, J.R. Williams, J. Appl. Phys. 98 (2005) 014902.
[21] M. Kumagawa, H. Kuwabara, S. Yamada, Jpn. J. Appl. Phys. 8 (1969) 421.
[22] J.M. Harris, H.C. Gatos, A.F. Witt, J. Electrochem. Soc. 116 (1969) 380.

[23] J.D. Hartman, A.M. Roskowski, Z.J. Reitmeier, K.M. Tracy, R.F. Davis, R.J. Nemanich, J. Vac. Sci. Technol. A 21 (2003) 394.
[24] J.D. Hartman, K. Naniwae, C. Petrich, R.J. Nemanich, R.F. Davis, Appl. Surf. Sci. 242 (2005) 428.
[25] H. Tsuchida, I. Kamata, K. Izumi, Appl. Phys. Lett. 70 (1997) 3072.
[26] H. Tsuchida, I. Kamata, K. Izumi, Jpn. J. Appl. Phys. 46 (1997) L699.
[27] H. Tsuchida, I. Kamata, K. Izumi, J. Appl. Phys. 85 (1999) 3569.
[28] N. Sieber, B.F. Mantel, Th. Seyller, J. Ristein, L. Ley, Diamond Relat. Mater. 10 (2001) 1291.
[29] N. Sieber, B.F. Mantel, Th. Seyller, J. Ristein, L. Ley, T. Heller, D.R. Batchelor, D. Schmeiber, Appl. Phys. Lett. 78 (2001) 1216.
[30] N. Sieber, T. Stark, Th. Seyller, L. Ley, C.A. Zorman, M. Mehregany, Appl. Phys. Lett. 80 (2002) 4726.
[31] N. Sieber, Th. Seyller, R. Graupner, L. Ley, R. Mikalo, P. Hoffman, D.R. Batchelor, D. Schmeiber, Appl. Surf. Sci. 184 (2001) 278.
[32] Th. Seyller, N. Sieber, T. Stark, L. Ley, C.A. Zorman, M. Mehregany, Surf. Sci. 532–535 (2003) 698.
[33] N. Sieber, Th. Seyller, L. Ley, D. James, J.D. Riley, R.C.G. Leckey, M. Polcik, Phys. Rev. B 67 (2003) 205304.
[34] B.I. Craig, P.V. Smith, Surf. Sci. 233 (1990) 255.
[35] L. Pizzagalli, A. Catellani, Surf. Sci. 494 (2001) 53.
[36] A. Catellani, L. Pizzagalli, G. Galli, Mater. Sci. Eng. B 96 (2002) 132.
[37] X. Peng, L. Ye, X. Wang, Surf. Sci. 571 (2004) 21.
[38] T. Balster, F.S. Tautz, H. Ibach, J.A. Schaefer, Diamond Relat. Mater. 6 (1997) 1353.
[39] H.W. Yeom, I. Matsuda, Y.-C. Chao, S. Hara, S. Yoshida, R.I.G. Uhrberg, Phys. Rev. B 61 (2000) 2417.
[40] S.M. Widstrand, L.S.O. Johansson, K.O. Magnusson, M.I. Larsson, H.W. Yeom, S. Hara, S. Yoshida, Surf. Sci. 479 (2001) 247.
[41] V. Derycke, P.G. Soukiassian, F. Amy, Y.J. Chabal, M.D. D'Angelo, H.B. Enriquez, M.G. Silly, Nat. Mater. 2 (2003) 253.
[42] F. Amy, Y.J. Chabal, J. Chem. Phys. 119 (2003) 6201.
[43] Th. Seyller, R. Graupner, N. Sieber, K.V. Emtsev, L. Ley, A. Tadich, J.D. Riley, R.C.G. Leckey, Phys. Rev. B 71 (2005) 245333.
[44] J.A. Dillon Jr., R.E. Schlier, H.E. Farnsworth, J. Appl. Phys. 30 (1959) 675.
[45] V. van Elsbergen, O. Janzen, W. Monch, Mater. Sci. Eng. B 46 (1997) 366.
[46] T. Fujino, T. Fuse, J.-T. Ryu, K. Inudzuka, Y. Yamazaki, M. Katayama, K. Oura, Appl. Surf. Sci. 169–170 (2001) 113.
[47] T. Aoyama, Y. Hisada, S. Mukainakano, A. Ichimiya, Jpn. J. Appl. Phys. 41 (2002) L174.
[48] Y. Hisada, T. Aoyama, S. Mukainakano, A. Ichimiya, Mater. Sci. Eng. B 96 (2002) 137.
[49] V. Derycke, P. Fonteneau, N.P. Pham, P. Soukiassian, Phys. Rev. B 63 (2001) 201305.
[50] C.R. Stoldt, C. Carraro, R. Maboudian, Surf. Sci. 466 (2000) 66.
[51] M.D. Allendorf, D.A. Outka, Surf. Sci. 258 (1991) 177.
[52] Y. Kim, D.R. Olander, Surf. Sci. 313 (1994) 399.
[53] J.M. Lannon Jr., J.S. Gold, C.D. Stinespring, J. Appl. Phys. 77 (1995) 3823.
[54] J.T. Law, J. Chem. Phys. 30 (1959) 1568.
[55] P. Kratzer, E. Pehlke, M. Scheffler, M.B. Raschke, U. Hofer, Phys. Rev. Lett. 81 (1998) 5596.
[56] G. Schulze, M. Henzler, Surf. Sci. 124 (1983) 336.
[57] C.C. Cheng, J.T. Yates Jr., Phys. Rev. B 43 (1991) 4041.
[58] J.J. Boland, Phys. Rev. Lett. 65 (1990) 3325.
[59] L.C. Feldman, P.J. Silverman, I. Stensgaard, Nucl. Instrum. Methods 168 (1980) 589.
[60] Z.H. Lu, K. Griffiths, P.R. Norton, T.K. Sham, Phys. Rev. Lett. 68 (1992) 1343.
[61] K. Oura, J. Yamane, K. Umezawa, M. Naitoh, F. Shoji, T. Hanawa, Phys. Rev. B 41 (1990) 1200.
[62] M. Watamori, M. Naitoh, H. Morioka, Y. Maeda, K. Oura, Appl. Surf. Sci. 82/83 (1994) 417.
[63] H. Froitzheim, U. Kohler, H. Lammering, Surf. Sci. 149 (1985) 537.
[64] H. Kobayashi, K. Edamoto, M. Onchi, M. Nishijima, J. Chem. Phys. 78 (1983) 7429.
[65] R.J. Culbertson, L.C. Feldman, P.J. Silverman, J. Vac. Sci. Technol. 20 (1982) 868.
[66] Ch. Kleint, K.-D. Brzoska, Surf. Sci. 231 (1990) 177.
[67] K.-D. Brzoska, Ch. Kleint, Thin Solid Films 34 (1976) 131.
[68] B.G. Koehler, C.H. Mak, D.A. Arthur, P.A. Coon, S.M. George, J. Chem. Phys. 89 (1988) 1709.
[69] G.A. Reider, U. Hofer, T.F. Heinz, Phys. Rev. Lett. 66 (1991) 1994.
[70] M.L. Wise, B.G. Koehler, P. Gupta, P.A. Coon, S.M. George, Surf. Sci. 258 (1991) 166.
[71] M.C. Flowers, N.B.H. Jonathan, Y. Liu, A. Morris, J. Chem. Phys. 102 (1995) 1034.
[72] M.C. Flowers, N.B.H. Jonathan, A. Morris, S. Wright, J. Chem. Phys. 108 (1998) 3342.
[73] K. Sinniah, M.G. Sherman, L.B. Lewis, W.H. Weinberg, J.T. Yates Jr., K.C. Janda, Phys. Rev. Lett. 62 (1989) 567.
[74] K. Sinniah, M.G. Sherman, L.B. Lewis, W.H. Weinberg, J.T. Yaters Jr., K.C. Janda, J. Chem. Phys. 92 (1990) 5700.
[75] U. Hofer, L. Li, T.F. Heinz, Phys. Rev. B 45 (1992) 9485.
[76] M.C. Flowers, N.B.H. Jonathan, Y. Liu, A. Morris, J. Chem. Phys. 99 (1993) 7038.
[77] D.-S. Lin, R.-P. Chen, Phys. Rev. B (1999) R8461.
[78] J.W. Sharp, G. Eres, Surf. Sci. 320 (1994) 169.
[79] L.A. Okada, M.L. Wise, S.M. George, Appl. Surf. Sci. 82 (/83) (1994) 410.
[80] C.M. Greenlief, M. Liehr, Appl. Phys. Lett. 64 (1994) 601.
[81] C.M. Greenlief, M. Armstrong, J. Vac. Sci. Technol. 13 (1995) 1810.
[82] X.F. Hu, Z. Xu, D. Lim, M.C. Downer, P.S. Parkinson, B. Gong, G. Hess, J.G. Ekerdt, Appl. Phys. Lett. 71 (1997) 1376.
[83] P. Gupta, V.L. Colvin, S.M. George, Phys. Rev. B 37 (1988) 8234.
[84] C.M. Greenlief, S.M. Gates, P.A. Holbert, Chem. Phys. Lett. 159 (1989) 202.
[85] A.V. Hamza, G.D. Kubiak, R.H. Stulen, Surf. Sci. 237 (1990) 35.
[86] L.H. Chua, R.B. Jackman, J.S. Foord, P.R. Chalker, C. Johnston, S. Romani, J. Vac. Sci. Technol. A 12 (1994) 3033.
[87] R.K. Gould, J. Chem. Phys. 63 (1975) 1825.
[88] Y.L. Yang, L.M. Struck, L.F. Sutcu, M.P. D'Evelyn, Thin Solid Films 225 (1993) 203.
[89] L.M. Struck, M.P. D'Evelyn, J. Vac. Sci. Technol. A 11 (1993) 1992.
[90] R.E. Thomas, R.A. Rudder, R.J. Markunas, J. Vac. Sci. Technol. A 10 (1992) 2451.
[91] M. McGonigal, M.L. Kempel, M.S. Hammond, K.D. Jamison, J. Vac. Sci. Technol. 14 (1996) 2308.
[92] C. Su, J.-C. Lin, Surf. Sci. 406 (1998) 149.
[93] Y.L. Yang, M.P. D'Eveyln, J. Vac. Sci. Technol. A 10 (1992) 978.
[94] B. Weiner, S. Skokov, M. Frenklach, J. Chem. Phys. 102 (1995) 5486.
[95] A. Hoffman, K. Bobrov, B. Fisgeer, H. Shechter, M. Folman, Diamond Relat. Mater. 5 (1996) 977.
[96] K. Bobrov, H. Schechter, M. Folman, A. Hoffman, Diamond Relat. Mater. 7 (1998) 170.
[97] Y. Mitsuda, T. Yamada, T.J. Chuang, H. Seki, R.P. Chin, J.Y. Huang, Y.R. Shen, Surf. Sci. 257 (1991) L633.
[98] C. Su, K.-J. Song, Y.L. Wang, H.-L. Lu, T.J. Chuang, J.-C. Lin, J. Chem. Phys. 107 (1997) 7543.
[99] R.P. Chin, J.Y. Huang, Y.R. Shen, T.J. Chuang, H. Seki, M. Buck, Phys. Rev. B 45 (1992) 1522.
[100] R.P. Chin, J.Y. Huang, Y.R. Shen, T.J. Chuang, H. Seki, Phys. Rev. B 52 (1995) 5985.
[101] B.F. Mantel, M. Stammler, J. Ristein, L. Ley, Diamond Relat. Mater. 9 (2000) 1032.
[102] A.V. Hamza, G.D. Kubiak, R.H. Stulen, Surf. Sci. 206 (1988) L833.
[103] K. Bobrov, B. Fisgeer, H. Shechter, M. Folman, A. Hoffman, Diamond Relat. Mater. 6 (1997) 736.
[104] M.T. Schulberg, C.A. Fox, G.D. Kubiak, R.H. Stulen, J. Appl. Phys. 77 (1995) 3484.
[105] D.D. Koleske, S.M. Gates, B.D. Thomas, J.N. Russell Jr., J.E. Butler, Surf. Sci. 320 (1993) L105.
[106] D.D. Koleske, S.M. Gates, B.D. Thomas, J.N. Russell Jr., J.E. Butler, J. Chem. Phys. 102 (1995) 992.
[107] M. Balooch, D.R. Olander, J. Chem. Phys. 63 (1975) 4772.
[108] V. Philipps, E. Vietzke, M. Erdweg, K. Flaskamp, J. Nucl. Mater. 145–147 (1987) 292.
[109] K. Ashida, K. Ichimura, M. Matsuyama, K. Watanabe, J. Nucl. Mater. 128–129 (1984) 792.
[110] K. Nakayama, S. Fukuda, T. Hino, T. Yamashina, J. Nucl. Mater. 145–147 (1987) 301.
[111] S. Fukuda, T. Hino, T. Yamashina, J. Nucl. Mater. 162–164 (1989) 997.
[112] J. Biener, A. Schenk, B. Winter, C. Lutterloh, U.A. Schubert, J. Kuppers, Surf. Sci. 307–309 (1994) 228.
[113] X. Jiang, W. Beyer, K. Reichelt, J. Appl. Phys. 68 (1990) 1378.
[114] C. Wild, P. Koidl, Appl. Phys. Lett. 51 (1987) 1506.
[115] B. Wood, H. Wise, J. Phys. Chem. 66 (1962) 1049.
[116] B. King, H. Wise, J. Phys. Chem. 67 (1962) 1163.
[117] H. Windischmann, J. Vac. Sci. Technol. A 9 (1991) 2459.
[118] H. Nagata, S. Yamaguchi, Y. Fujino, M. Hirabayashi, K. Kamada, J. Nucl. Mater. 128–129 (1984) 760.
[119] Y. Oya, Y. Onishi, H. Kodama, K. Okuno, S. Tanaka, J. Nucl. Mater. 337–339 (2005) 595.
[120] D. Keroack, B. Terreault, J. Vac. Sci. Technol. A 14 (1996) 3130.
[121] T. Sugiyama, Y. Morimoto, K. Iguchi, K. Okuno, M. Miyamoto, H. Iwakiri, N. Yoshida, J. Nucl. Mater. 307–311 (2002) 1080.
[122] M. Mayer, M. Balden, R. Behrisch, J. Nucl. Mater. 252 (1998) 55.
[123] S.W. King, R.J. Nemanich, R.F. Davis, J. Electrochem. Soc. 146 (1999) 2648.
[124] S.W. King, M. Busby, C. Ronning, R.J. Nemanich, R.F. Davis, J. Appl. Phys. 84 (1998) 6042.
[125] S.W. King, R.S. Kern, M.C. Benjamin, J.P. Barnak, R.J. Nemanich, R.F. Davis, J. Electrochem. Soc. 146 (1999) 3448.
[126] J. van der Weide, Ph.D. dissertation North Carolina State University, 1994.
[127] S.W. King, E.P. Carlson, R.J. Therrien, J.A. Christman, R.J. Nemanich, R.F. Davis, J. Appl. Phys. 86 (1999) 5584.
[128] J.B. Miller, H.R. Siddiqui, S.M. Gates, J.N. Russell Jr., J.T. Yates Jr., J.C. Tully, M.J. Cardillo, J. Chem. Phys. 87 (1987) 6725.
[129] D. Parker, M. Jones, B. Koel, Surf. Sci. 233 (1990) 65.
[130] Perkin Elmer Auger Electron Spectroscopy Handbook.
[131] H.R. Han, L.D. Schmidt, J. Phys. Chem. 75 (1971) 227.
[132] R. Bafrali, A.T. Bell, Surf. Sci. 278 (1992) 353.
[133] J.A. Prybyla, P.J. Estrup, Surf. Sci. 290 (1993) 413.
[134] G.P. Lopinski, J.A. Prybyla, P.J. Estrup, Surf. Sci. 315 (1994) 269.
[135] D.E. Shleifman, D. Shaltiel, I.T. Steinberger, J. Alloy Comp. 223 (1995) 81.
[136] U. Starke, J. Schardt, J. Bernhardt, M. Franke, K. Reuter, H. Wedler, K. Heinz, Phys. Rev. Lett. 80 (1998) 758.
[137] J. Schardt, J. Bernhardt, U. Starke, K. Heinz, Phys. Rev. B 62 (2000) 10335.
[138] S.M. Gates, C.M. Greenlief, D.B. Beach, P.A. Holbert, J. Chem. Phys. 92 (1990) 3144.

[139] S.M. Gates, S.K. Kulkarni, Appl. Phys. Lett. 60 (1992) 53.
[140] J. Abrefah, D.R. Olander, Surf. Sci. 209 (1989) 291.
[141] S.M. Gates, R.R. Kunz, C.M. Greenlief, Surf. Sci. 207 (1989) 364.
[142] H. Kim, G. Glass, S. Park, T. Spila, N. Taylor, J. Abelson, J. Greene, Appl. Phys. Lett. 69 (1996) 3869.
[143] Y. Foo, K. Bratland, B. Cho, J. Soares, P. Desjardins, J. Greene, Surf. Sci. 513 (2002) 475.
[144] B. Ning, J. Crowell, Surf. Sci 295 (1993) 79.
[145] N.M. Russell, J.G. Ekerdt, Surf. Sci. 369 (1996) 51.
[146] H. Kim, N. Taylor, J. Abelson, J. Greene, J. Appl. Phys. 82 (1997) 6062.
[147] D. Eres, J.W. Sharp, Appl. Phys. Lett. 60 (1992) 2764.
[148] L. Surnev, M. Tikhov, Surf. Sci. 138 (1984) 40.
[149] G. Eres, J.W. Sharp, J. Vac. Sci. Technol. A 11 (1993) 2463.
[150] M.P. D'Evelyn, S.M. Cohen, E. Rouchouze, Y.L. Yang, J. Chem. Phys. 98 (1993) 3560.
[151] L. Lewis, J. Segall, K. Janda, J. Chem. Phys. 102 (1995) 7222.
[152] J. Lee, J. Maeng, A. Kim, Y. Cho, S. Kim, J. Chem. Phys. 118 (2003) 1929.
[153] H. Nakazawa, M. Suemitsu, Appl. Surf. Sci. 162–163 (2000) 139.
[154] J. Furthmuller, F. Bechstedt, H. Husken, B. Schroter, W. Richter, Phys. Rev. B 58 (1998) 13712.
[155] L.S.O. Johansson, L. Duda, M. Laurenzis, M. Krieftewirth, B. Reihl, Surf. Sci. 445 (2000) 109.
[156] C. Benesch, M. Fartmann, H. Merz, Phys. Rev. B 64 (2001) 205314.
[157] R. Ostendorf, K. Wulff, C. Benesch, H. Zacharias, Surf. Sci. 600 (2006) 3839.
[158] K.V. Emtsev, Th. Seyller, L. Ley, A. Tadich, L. Broekman, J.D. Riley, R.C.G. Leckey, M. Preuss, Surf. Sci. 600 (2006) 3845.
[159] J.E. Northrup, J. Neugebauer, Phys. Rev. B 57 (1998) R4230.
[160] M. Sabisch, P. Kruger, J. Pollman, Phys. Rev. B 55 (1997) 10561.
[161] V. Bermudez, J. Long, Appl. Phys. Lett. 66 (1995) 475.
[162] L. Wenchang, Y. Weidong, Z. Kaiming, J. Phys. D 3 (1991) 9079.